

University of Massachusetts Medical School

eScholarship@UMMS

University of Massachusetts Medical School Faculty Publications

2020-10-20


Coxsackievirus B Type 4 Infection in beta Cells Downregulates the Chaperone Prefoldin URI to Induce a MODY4-like Diabetes via Pdx1 Silencing

Hugo Bernard
National Cancer Research Center

Et al.

Let us know how access to this document benefits you.

Follow this and additional works at: https://escholarship.umassmed.edu/faculty_pubs

 Part of the [Cellular and Molecular Physiology Commons](#), [Endocrine System Diseases Commons](#), [Endocrinology Commons](#), [Hormones, Hormone Substitutes, and Hormone Antagonists Commons](#), [Nutritional and Metabolic Diseases Commons](#), and the [Viruses Commons](#)

Repository Citation

Bernard H, Teijeiro A, Chaves-Perez A, Perna C, Satish B, Novials A, Wang JP, Djouder N. (2020). Coxsackievirus B Type 4 Infection in beta Cells Downregulates the Chaperone Prefoldin URI to Induce a MODY4-like Diabetes via Pdx1 Silencing. University of Massachusetts Medical School Faculty Publications. <https://doi.org/10.1016/j.xcrm.2020.100125>. Retrieved from https://escholarship.umassmed.edu/faculty_pubs/1855

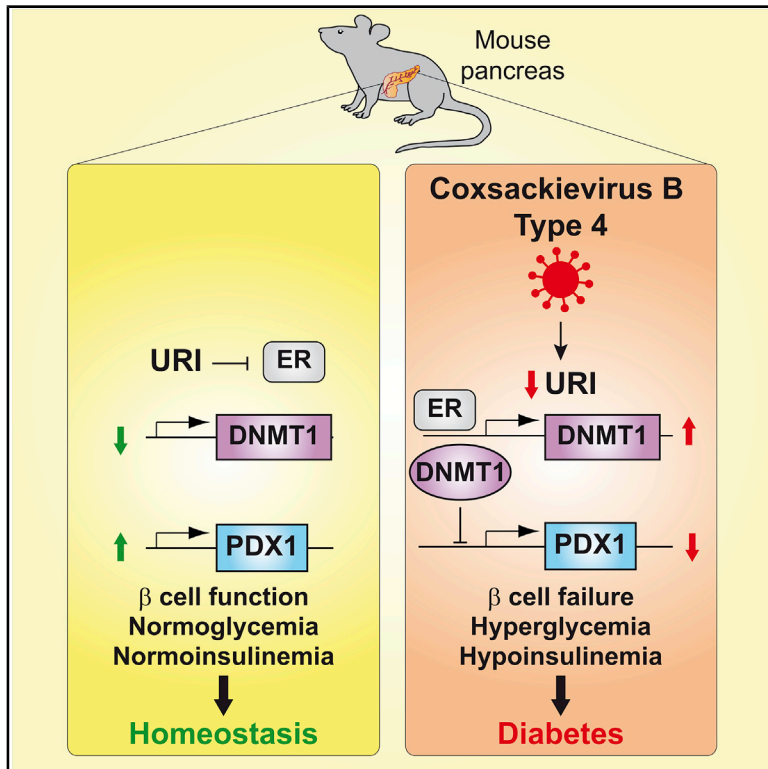
Creative Commons License



This work is licensed under a [Creative Commons Attribution-NonCommercial-No Derivative Works 4.0 License](#). This material is brought to you by eScholarship@UMMS. It has been accepted for inclusion in University of Massachusetts Medical School Faculty Publications by an authorized administrator of eScholarship@UMMS. For more information, please contact Lisa.Palmer@umassmed.edu.

Coxsackievirus B Type 4 Infection in β Cells Downregulates the Chaperone Prefoldin URI to Induce a MODY4-like Diabetes via *Pdx1* Silencing

Graphical Abstract



Authors

Hugo Bernard, Ana Teijeiro, Almudena Chaves-Pérez, ..., Anna Novials, Jennifer P. Wang, Nabil Djouder

Correspondence

ndjouder@cniio.es

In Brief

Bernard et al. provide a molecular link between viral infection and diabetes. The authors show that infection of pancreatic β cells with the enterovirus coxsackievirus B type 4 downregulates the molecular co-chaperone URI, which leads to DNMT1-mediated *Pdx1* silencing and, subsequently, to a MODY4-like diabetes.

Highlights

- Coxsackievirus B type 4 infection downregulates URI and affects β cell function
- Genetic URI ablation in mouse pancreas recapitulates diabetes
- URI controls *Pdx1* methylation via ER α -activating DNMT1
- Coxsackievirus B type 4, URI, PDX1, and DNMT1 expression correlate in human pancreata



Article

Coxsackievirus B Type 4 Infection in β Cells Downregulates the Chaperone Prefoldin URI to Induce a MODY4-like Diabetes via *Pdx1* Silencing

Hugo Bernard,¹ Ana Teijeiro,^{1,5} Almudena Chaves-Pérez,^{1,5} Cristian Perna,² Basanthi Satish,³ Anna Novials,⁴ Jennifer P. Wang,³ and Nabil Djouder^{1,6,*}

¹Molecular Oncology Programme, Growth Factors, Nutrients and Cancer Group, Centro Nacional de Investigaciones Oncológicas, CNIO, Madrid 28029, Spain

²Department of Pathology, Hospital Universitario Ramón y Cajal, IRYCIS, Madrid 28034, Spain

³Department of Medicine, University of Massachusetts Medical School, Worcester, Massachusetts, USA

⁴IDIBAPS, August Pi i Sunyer Biomedical Research Institute and, CIBERDEM, Spanish Biomedical Research Centre in Diabetes and Associated Metabolic Disorders, Barcelona, Spain

⁵These authors contributed equally

⁶Lead Contact

*Correspondence: ndjouder@cnio.es

<https://doi.org/10.1016/j.xcrm.2020.100125>

SUMMARY

Enteroviruses are suspected to contribute to insulin-producing β cell loss and hyperglycemia-induced diabetes. However, mechanisms are not fully defined. Here, we show that coxsackievirus B type 4 (CVB4) infection in human islet-engrafted mice and in rat insulinoma cells displays loss of unconventional prefoldin RPB5 interactor (URI) and PDX1, affecting β cell function and identity. Genetic URI ablation in the mouse pancreas causes PDX1 depletion in β cells. Importantly, diabetic PDX1 heterozygous mice overexpressing URI in β cells are more glucose tolerant. Mechanistically, URI loss triggers estrogen receptor nuclear translocation leading to DNA methyltransferase 1 (DNMT1) expression, which induces *Pdx1* promoter hypermethylation and silencing. Consequently, demethylating agent procainamide-mediated DNMT1 inhibition reinstates PDX1 expression and protects against diabetes in pancreatic URI-depleted mice. Finally, the β cells of human diabetes patients show correlations between viral protein 1 and URI, PDX1, and DNMT1 levels. URI and DNMT1 expression and PDX1 silencing provide a causal link between enterovirus infection and diabetes.

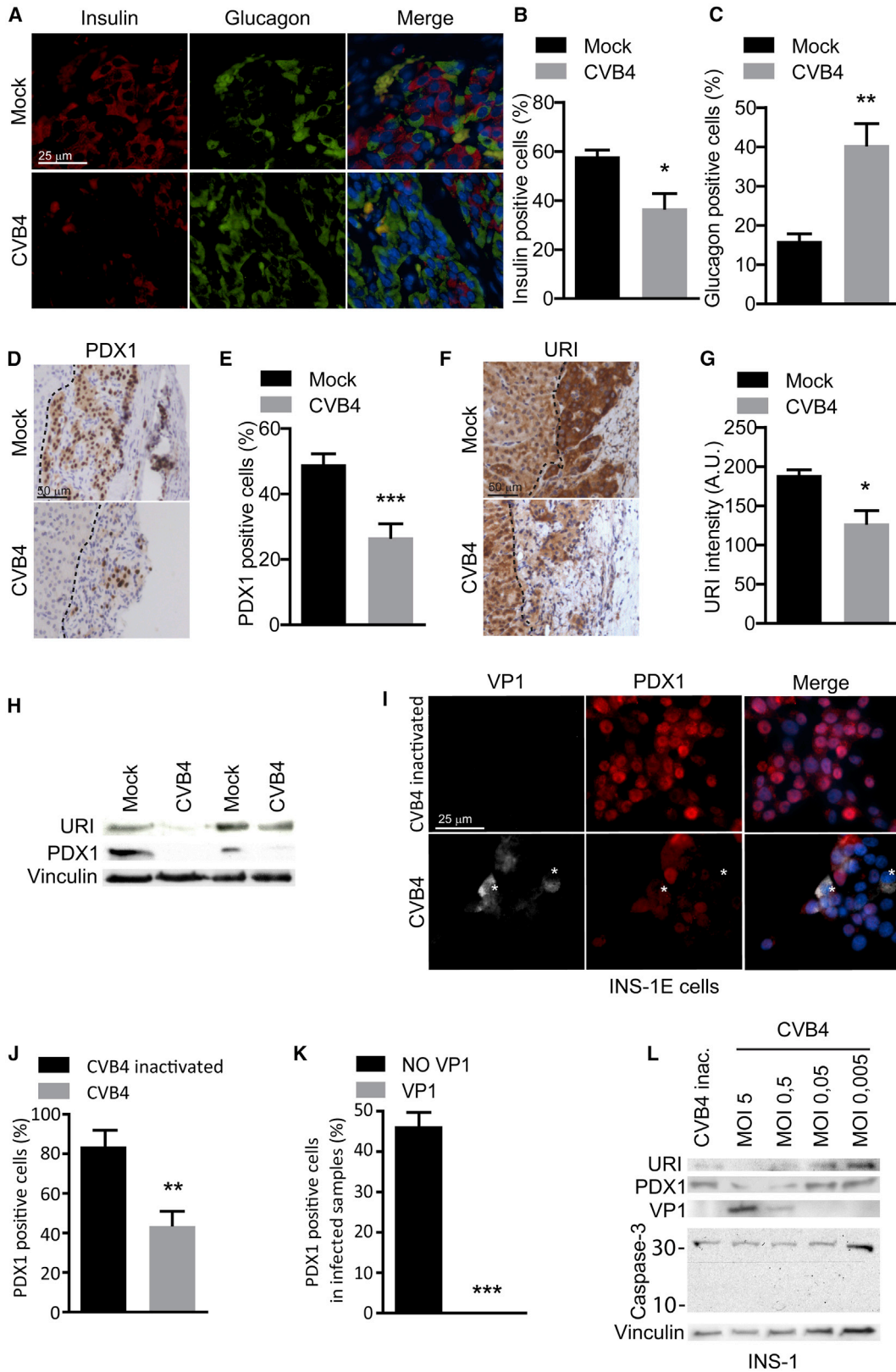
INTRODUCTION

Glucose homeostasis is maintained through tight dynamic regulation of insulin expression by pancreatic β cells, dysfunction or alteration of which can lead to high blood sugar, and hence type 1 or 2 diabetes mellitus (T1D or T2D) or maturity-onset diabetes of the young (MODY).^{1–3} Notably, T1D is attributed to β cell-specific antibodies (first-line predictive and diagnostic markers) and T cell-mediated autoimmune responses. However, the presence of autoantibodies is not always accompanied by symptoms and the presence of immune-infiltrated cells in the endocrine pancreas of T1D patients, as for instance in idiopathic T1D, characterized by an almost complete insulin deficiency without evidence of autoimmune responses.^{4,5} Moreover, the susceptibility of antigen recognition through polymorphisms in the human leukocyte antigen (HLA) loci within the major histocompatibility complex, which accounts for half of the susceptibility risk of T1D, does not explain the steep increase in T1D prevalence that has occurred in the last 30 years.² Low heritability suggests that T1D is probably modulated by environmental factors.¹ For example, early-onset obesity increases the glucose-sensing

threshold for insulin production,^{6,7} suggesting that nutrient overload can promote T1D (probably the idiopathic type), and some pathological agents have suggested causal responsibility.^{8,9} Moreover, it has been recently proposed that viral transcription factors operating across risk loci within disease phenotypes may play major roles in autoimmune disorders.¹⁰ Accordingly, several studies suggest that enteroviruses (particularly coxsackievirus serotypes) may be critical triggers of T1D, either through direct cytolytic effects and gradual β cell destruction or bystander activation of other factors participating in the T1D process.^{1,2,8,11–13} More important, fresh pancreatic tissue analysis of patients with new-onset T1D has revealed the presence of enterovirus-positive cells in the endocrine compartment advocating for an etiological role of viral infection in T1D.¹⁴ In this context, antiviral drugs and vaccine trials have been proposed for the prevention of T1D.¹⁵ However, the mechanisms through which β cell alterations induced by viral infections can affect insulin production remain unknown.

Pancreatic and duodenal homeobox 1 (PDX1) is a core transcription factor responsible for pancreatic development, including β cell maturation and duodenal differentiation. β cell-





(legend on next page)

selective disruption of *Pdx1* in mice leads to the development of diabetes,¹⁶ and mutations in PDX1 can cause a monogenic form of diabetes (MODY4) in humans.¹⁷ In addition, PDX1 plays a major role in maintaining β cell function and identity.^{18,19} Interestingly, longitudinal analyses of metabolic parameters in T1D patients identified β cell dysfunction 5 years before diagnosis.²⁰ Moreover, *PDX1* mRNA expression is decreased in coxsackievirus B type 4 (CVB4)-infected human pancreatic samples.^{11,21,22} However, the molecular mechanisms of PDX1 alterations in diabetes linked to CVB4 infection remain elusive.

The molecular co-chaperone unconventional prefoldin RPB5 interactor (URI) is a nutrient- and stress-sensing protein maintaining cellular homeostasis.^{23–25} URI controls the activity of the β -linked *N*-acetylglucosamine (O-GlcNAc) transferase OGT to regulate protein O-GlcNAcylation, conferring survival mechanisms.²⁶ In this regard, increased protein O-GlcNAcylation is directly linked to insulin resistance and hyperglycemia-induced glucose toxicity.²⁷ In addition, URI expression in hepatocytes induces diabetes and non-alcoholic steatohepatitis.²⁸ URI expression reportedly binds and sequesters in the cytoplasm the aryl hydrocarbon (AhR)- and estrogen receptor (ER), inhibiting their nuclear transcriptional activity, causing NAD⁺ depletion and liver cancer.²⁹ Interestingly, cytoplasmic ER is linked to better glucose homeostasis by maintaining β cell survival in mice.³⁰ Moreover, gender-specific differences in glucose homeostasis reveal that sex hormones may play a role in the development of diabetes.³¹ Recent data also suggest that ER gene polymorphism affects the age of onset of T1D.³² Whether URI plays a role in β cell identity and diabetes still needs to be determined.

Here, we demonstrate that CVB4 infection in human islets engrafted into mice and a rat insulinoma cell line causes the downregulation of URI and PDX1, affecting β cell function and identity. *Uri*^{flox/flox}; *Pdx1-cre* mice, with pancreatic URI ablation, show PDX1 loss in β cells and recapitulate clinical diabetes features. Interestingly, pre-diabetic PDX1 heterozygous mice overexpressing URI in β cells are more glucose tolerant. Mechanistically, we show that URI depletion triggers ER nuclear translocation, leading to DNA methyltransferase 1 (DNMT1) expression and causing *Pdx1* promoter hypermethylation and silencing. Treating *Uri*^{flox/flox}; *Pdx1-cre* mice with the demethylating agent procainamide reinstates PDX1 expression and protects against

diabetes. Finally, the β cells of human T1D and T2D patients show URI, PDX1, and DNMT1 expression patterns similar to those observed with CVB4 infection. Overall, our findings delineate an unappreciated circuit in which CVB4 infection can lead to diabetes through URI loss, causing *Pdx1* silencing by DNMT1-induced hypermethylation.

RESULTS

CVB4 Infection Causes URI Loss and Affects β Cell Function and Identity

CVB4 exhibits selective tropism toward the pancreas, particularly β cells in humans, which express its receptor.³³ Neither CVB3 nor CVB4 infection of C57BL/6 mouse islets consistently results in diabetes, and the efficiency of the replication of these viruses seems to be controversial and context dependent in mice.³⁴ We therefore used human islets infected with CVB4 and engrafted in immunodeficient mice¹¹ in the experiments reported here. At time of death, CVB4-infected mice presented hypoinsulinemia and low C-peptide levels, and >40% had developed hyperglycemia¹¹ (Figures S1A and S1B; Table S1). The quantification of insulin and glucagon immunofluorescent cells in non-infected and CVB4-infected human grafts showed that the proportion of insulin-producing cells significantly decreased in infected samples and the proportion of glucagon-producing cells increased (Figures 1A–1C), despite no significant differences in the signal intensity of insulin and glucagon, as shown by immunofluorescence (IF) (Figures S1C and S1D). This suggests the loss of β cell identity and the conversion of β cells to glucagon-producing α cells,³⁵ a phenomenon that is associated with PDX1 depletion.¹⁸ Thus, PDX1 is critical for β cell maintenance and insulin production.¹⁸ As reported for the loss of β cell identity, immunohistochemistry (IHC) analyses showed that the percentage of PDX1⁺ cells was significantly lower in virally infected human grafts than in non-infected samples (Figures 1D, 1E, and S1E).

Interestingly, URI expression was downregulated in CVB4-infected samples compared to non-infected samples (Figures 1F and 1G). Next, we analyzed human primary islets infected (or not) with CVB4 *ex vivo*.¹¹ Western blot (WB) revealed that CVB4 infection caused the downregulation of PDX1 and URI at 48 h post-infection (Figure 1H). IF analysis demonstrated that

Figure 1. CVB4 Infection Causes URI Loss and Affects β Cell Function and Identity

- (A) Immunofluorescence (IF) of insulin and glucagon from human islet xenografts in CVB4- or mock-infected mice.
 (B and C) Quantification of the proportion of insulin (B)- and glucagon (C)-positive cells. At least 100 cells in the pancreatic grafts were counted per field, with up to 5 fields per sample (n = 10 and 7).
 (D) Immunohistochemistry (IHC) of PDX1 from CVB4-infected human islet xenografts in mice. The dotted outlines represent the limit between the kidney and the human graft.
 (E) Quantification of PDX1⁺ cells (n = 10 and 7).
 (F) IHC of URI from CVB4- or mock-infected human islet xenografts in mice.
 (G) Quantification of URI staining intensity (n = 10 and 7).
 (H) Western blot (WB) of URI, PDX1, and vinculin in CVB4- or mock-infected primary human islets (representative blot from 2 donors).
 (I) IF of viral protein 1 (VP1) and PDX1 in INS-1E cells infected with CVB4 (or inactivated CVB4). Asterisk denotes CVB4-infected cells.
 (J) Quantification of PDX1⁺ INS-1E cells infected with CVB4 or inactivated CVB4. At least 100 cells per field and 3 fields per samples were counted (N = 3).
 (K) Quantification of PDX1 nuclear-positive cells from VP1⁺ cells (VP1) and VP1⁻ cells (NO VP1) in CVB4-infected INS-1E cells. At least 100 cells per field and 3 fields per sample were counted (N = 3).
 (L) WB of URI, PDX1, caspase-3, and vinculin in INS-1 cells infected with CVB4 (MOI 5, 0.5, 0.05, and 0.005) or inactivated CVB4.
 Data are means \pm SEMs. Statistical analysis done using Student's t test. *p < 0.05; **p < 0.01; ***p < 0.001. Scale bars, 50 μ m in (D) and (F); 25 μ m in (A) and (I).

the number of PDX1⁺ cells was decreased, although the percentage of glucagon-positive cells remained unchanged (Figures S1F–S1H). Since human primary islets are a relevant source of material but at the same time limited in amount and manipulability, we decided to pursue our investigations in the INS-1E and INS-1 rat insulinoma cell lines.³⁶ Notably, INS-1E cells are a clonal cell line of INS-1 with higher insulin sensitivity. IF in INS-1E cells confirmed that CVB4 particles decreased the total number of PDX1 cells 48 h post-infection when compared to cells infected with inactivated viruses, whereas none of the infected cells were PDX1⁺ (Figures 1I–1K). Moreover, WB analysis indicated that URI and PDX1 were dose-dependently downregulated in CVB4-infected INS-1E and INS-1 cells, without any remarkable signs of viral cytotoxic effects (no cell death was detected) (Figures 1L and S1I–S1K). Notably, CVB4 expression was detected by staining viral protein 1 (VP1), a component of the coxsackievirus family found in human T1D samples, and the antibody specificity of which was previously characterized.^{37,38} Interestingly, human URI overexpression in CVB4-infected INS-1 cells showed nuclear PDX1 expression (Figure S1L). These data indicate that CVB4 infection causes URI and PDX1 downregulation, possibly affecting β cell identity and function, independent of viral cytotoxicity. Thus, URI loss may be a CVB4-mediated trigger of disease and participate in the “viral paradigm” of diabetes.

Genetic URI Ablation in Mouse Pancreas Leads to Glucose Intolerance and Premature Death

To further explore the consequences of URI loss in the pancreas, we generated a genetic model of URI ablation in murine pancreas by crossing *Uri1* floxed mice with transgenic mice expressing Cre recombinase under control of the *Pdx1* promoter, which is induced during embryonic development (E8.5),³⁹ obtaining *Pdx1-cre* and *Uri1^{flox/flox}; Pdx1-cre* mice (Figure S2A). IHC and WB analyses indicated that URI was specifically downregulated in the pancreases of *Uri1^{flox/flox}; Pdx1-cre* mice, but not in their other organs (Figures S2B–S2D). Crossing URI *Uri1^{flox/flox}; Pdx1-cre* with the reporter line R26-stop-enhanced yellow fluorescent protein (EYFP)⁴⁰ confirmed the specific expression of EYFP, and consequently, the absence of URI-expressing cells in the pancreatic islets, as shown by EYFP⁺ signals by IHC (Figures S2E and S2F).

Uri1^{flox/flox}; Pdx1-cre mice had reduced survival, dying quickly after adulthood. Notably, 50% of males died within 15 weeks of birth, whereas females died later (Figures 2A and S2G). At 7 weeks of age, *Uri1^{flox/flox}; Pdx1-cre* males displayed reduced pancreas weights, hyperglycemia, and hyperinsulinemia at fasting (Figures 2B–2D). In addition, glucose intolerance was detected in *Uri1^{flox/flox}; Pdx1-cre* males and females after 6 h of fasting (Figures 2E and S2H) and insulin secretion was reduced in *Uri1^{flox/flox}; Pdx1-cre* mice when compared to their control littermates (Figure 2F). No significant differences in insulin sensitivity were detected between *Uri1^{flox/flox}; Pdx1-cre* males and females (Figures S2I and S2J), and total amounts of pancreatic insulin were lower in *Uri1^{flox/flox}; Pdx1-cre* mice than in control littermates (Figure 2G). Furthermore, β cell density was higher (Figures 2H and 2I), but β cell mass and average pancreatic islet size were significantly lower (Figures 2J and 2K) in *Uri1^{flox/flox}; Pdx1-*

cre mice than in littermate controls, even though Ki67 and cleaved caspase 3 staining, respectively, indicated that proliferation and apoptosis were not affected in *Uri1^{flox/flox}; Pdx1-cre* mice (Figures S2K and S2L), corroborating the non-cytotoxic effects shown with CVB4 infections¹¹ (Figures S1L–S1K). Thus, *Uri1^{flox/flox}; Pdx1-cre* mice present a drastic β cell compartment alteration, with features resembling an idiopathic T1D or a MODY-like diabetes, highly reminiscent of MODY4 (Figure 2L).

URI Controls PDX1 Expression and β Cell Identity in Mice

We next analyzed the expression of PDX1 following URI depletion. Since the *Uri1^{flox/flox}; Pdx1-cre* phenotype was more pronounced in males than in females, we focused the following study on male mice. WB analysis revealed that PDX1 expression was significantly decreased in the pancreases of *Uri1^{flox/flox}; Pdx1-cre* mice, but not in their littermate controls, while IF staining in pancreatic islets showed the downregulation of PDX1 in β cells (Figures 3A and S3A–S3C). Quantitative reverse transcriptase-PCR (qRT-PCR) analyses of pancreatic samples indicated that PDX1 target genes *Ins-1* and *Ins-2* were downregulated in *Uri1^{flox/flox}; Pdx1-cre* mice (Figure 3B), confirming that PDX1 expression is altered in *Uri1^{flox/flox}; Pdx1-cre* pancreases. In addition, we observed the downregulation of *Pdx1* gene expression in INS-1E cells after URI downregulation using specific small interfering RNA (siRNA) against URI (siURI) (Figure S3D). Notably, WB analysis of the duodenum indicated that the expression of PDX1 was halved in *Uri1^{flox/flox}; Pdx1-cre* mice but no differences were detected in intestinal architecture and permeability (Figures S3E–S3G). Moreover, PDX1 was not expressed in the ileum as shown by WB (Figure S3E). Therefore, the effects seen in *Uri1^{flox/flox}; Pdx1-cre* mice may be caused by URI-mediated PDX1 regulation in the pancreatic islets.

The above results suggest that the effects observed in *Uri1^{flox/flox}; Pdx1-cre* mice may be caused by the loss of pancreatic PDX1. Since PDX1 is crucial for the development and maintenance of pancreatic lineages, the β cell compartment in *Uri1^{flox/flox}; Pdx1-cre* mice may not have developed and matured properly, resulting in the inadequate production of insulin and control of glycemia. We therefore analyzed pancreases of 2-day-old *Uri1^{flox/flox}; Pdx1-cre* mice. IF analysis showed that they had reduced PDX1 and insulin levels (Figures 3C–3F). Moreover, like 7-week-old *Uri1^{flox/flox}; Pdx1-cre* mice, 2-day-old mice had significantly smaller pancreatic islets (with lower organosomatic indices) and higher blood glucose levels than littermate controls (Figures 3G–3I). At this stage, *Uri1^{flox/flox}; Pdx1-cre* mice did not show any deviations in β cell density (Figure S3H), suggesting that alterations in the endocrine compartment are still to come. Thus, URI deletion may affect pancreas homeostasis via PDX1 downregulation.

Notably, blood glucagon levels were significantly increased in 7-week old *Uri1^{flox/flox}; Pdx1-cre* mice, while their α cell identity was maintained, according to qRT-PCR analyses of *Glucagon* and *Arx-1* (Figures 3J and S3I), despite the dramatic loss of the endocrine compartment observed in *Uri1^{flox/flox}; Pdx1-cre* mice. Forcing PDX1 expression can also convert a small proportion of α cells into β cells.⁴¹ In addition, the endogenous reprogramming of α cells into β cells, induced by viral gene therapy that

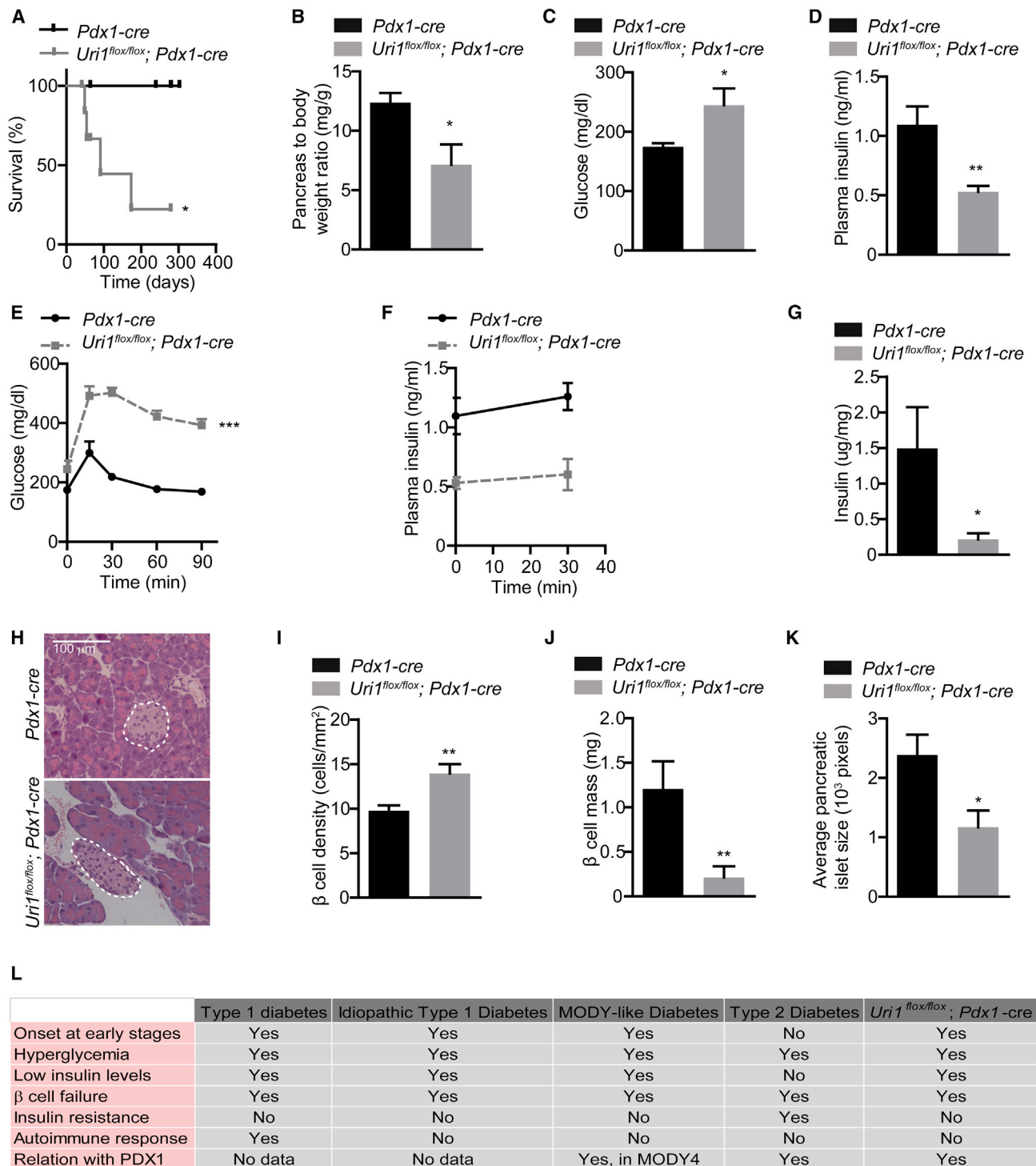


Figure 2. Genetic URI Ablation in Mouse Pancreas Leads to Glucose Intolerance and Premature Death

- (A) Survival curve of *Pdx1-cre* and *Uri1^{fllox/fllox}; Pdx1-cre* males (n = 10 and 7).
 (B) Organosomatic index of 7-week-old *Pdx1-cre* and *Uri1^{fllox/fllox}; Pdx1-cre* pancreases (n = 9 and 6).
 (C) Fasting glucose levels of 7-week-old *Pdx1-cre* and *Uri1^{fllox/fllox}; Pdx1-cre* males (n = 10 and 7).
 (D) Fasting plasma insulin levels in 7-week-old *Pdx1-cre* and *Uri1^{fllox/fllox}; Pdx1-cre* mice (n = 8 and 5).
 (E and F) Glucose tolerance and insulin secretion tests in 7-week-old *Pdx1-cre* and *Uri1^{fllox/fllox}; Pdx1-cre* mice (n = 10 and 7).
 (G) Pancreatic insulin levels in 7-week-old *Pdx1-cre* and *Uri1^{fllox/fllox}; Pdx1-cre* mice (n = 12 and 4).

(legend continued on next page)

reinstates PDX1 expression, can reportedly reverse autoimmune diabetes in both β cell-toxin-induced diabetic mice and autoimmune non-obese diabetic (NOD) mice, a unique animal model of T1D.⁴² Moreover, following experimental β cell ablation, α and δ cells can be converted into insulin-producing cells acquiring β cell properties.^{43–46} More important, recent findings suggest that CVB4 infection of human primary pancreatic ductal cell cultures impairs differentiation into insulin-producing cells.⁴⁷ We therefore checked for the presence of polyhormonal cells (secreting glucagon and insulin), a phenomenon partly mediated by the loss of PDX1.⁴³ Significantly, confocal images of *Uri1^{lox/lox}*; *Pdx1-cre* pancreatic islets showed increased polyhormonal cells (Figures S3K and S3L).

Next, we investigated whether CVB4 infection could be directly responsible for the loss of β cell identity and the transdifferentiation into insulin-glucagon bihormonal cells.⁴⁸ Confocal co-IF of insulin and glucagon revealed the presence of bihormonal cells in CVB4-infected human islet grafts (Figures 3M and 3N), suggesting that viral infection induces the reprogramming of hormonal cells.³⁵ In addition, we did triple staining for insulin, glucagon, and VP1.^{8,9} Results demonstrated that β cell-specific tropism of CVB4 viruses favored bihormonal cell apparition (Figures S3J and S3K). Strikingly, we could not observe any infected cells expressing nuclear PDX1—only some remaining cytoplasmic expression (Figure S3K). Moreover, gene expression analysis in CVB4-infected human primary islets indicated that β cell (*INS*, *NKX6-1*, and *PDX1*) transcripts were downregulated and α cell (*ARX* and *GCG*)-specific markers were upregulated (Figure S3L). These data indicate that CVB4 causes URI downregulation, affecting β cell identity and function, possibly through PDX1 loss.

URI Is Required to Maintain Glucose Homeostasis by Regulating PDX1 Expression

We have surmised that URI is required to maintain glycemia in conditions in which β cell functions are altered. Accordingly, we generated a knockin mouse (designated *hURI1^(+/KI)*; *Pdx1^(tTA/+)*) expressing FLAG-tagged human URI (*hURI1*) via a tetracycline-dependent transactivator (tTA(OFF)) that has replaced the coding region of the endogenous *Pdx1* gene to ensure correct temporal and spatial expression of the regulatable transactivator (tTA(OFF): *Pdx1^(tTA/+)* mouse) (Figure S4A).⁴⁹ In the absence of doxycycline, *hURI1^(+/KI)*; *Pdx1^(tTA/+)* mice expressed hURI specifically in β cells from a single allele from embryonic development (Figures S4B–S4D). More important, *hURI1^(+/+)*; *Pdx1^(tTA/+)* littermates lacked hURI expression and displayed a pre-diabetic phenotype, likely due to the disruption of one *Pdx1* allele and reduced PDX1 levels.⁴⁹ IF analysis showed that *hURI1^(+/KI)*; *Pdx1^(tTA/+)* mice had higher PDX1 expression than littermate controls with only the *Pdx1^(tTA/+)* allele (Figures 4A–4C). In addition, hURI-expressing *Pdx1*-tTA mice (*hURI1^(+/KI)*; *Pdx1^(tTA/+)* mice) displayed better glucose clearance

than the pre-diabetic *hURI1^(+/+)*; *Pdx1^(tTA/+)* mice (Figures 4D and S4E), although *hURI1^(+/KI)*; *Pdx1^(tTA/+)* mice displayed the same fasting or post-prandial glucose levels and similar fasting insulin levels (Figures S4F and S4G). *hURI1^(+/KI)*; *Pdx1^(tTA/+)* mice had better insulin secretion, but no differences in insulin sensitivity between them, and the pre-diabetic mice were detected (Figures 4E, S4H, and S4I). IF and transmission electron microscopy (TEM) analyses of β cells, respectively, indicated that insulin levels and numbers of insulin secretion granules were significantly increased in *hURI1^(+/KI)*; *Pdx1^(tTA/+)* mice (Figures 4F–4H). Notably, no changes in their β and α cell densities were observed, but β cell mass and proliferation were also enhanced; apoptosis was not observed in *hURI1^(+/KI)*; *Pdx1^(tTA/+)* mice, however (Figures S4J–S4N). Consistent with increased insulin content, insulin secretion tests in isolated islets of *hURI1^(+/KI)*; *Pdx1^(tTA/+)* mice showed increased secretion after 30 min of stimulation by glucose, potassium chloride (KCl), tolbutamide, or forskoline (Figure 4I). Crosses of *Uri1^{lox/lox}*; *Pdx1-cre* and *hURI1^(+/KI)*; *Pdx1^(tTA/+)* mice had better glucose clearance than *Uri1^{lox/lox}*; *Pdx1-cre* and *hURI1^(+/+)*; *Pdx1^(tTA/+)* mice (Figure 4J). *hURI1^(+/KI)*; *Pdx1^(tTA/+)*; *Uri1^{lox/lox}*; *Pdx1-cre* mice also had normal survival parameters, while *hURI1^(+/+)*; *Pdx1^(tTA/+)*; *Uri1^{lox/lox}*; *Pdx1-cre* controls died before birth (Figure 4K), indicating that URI is required to maintain glucose homeostasis by regulating PDX1 expression.

Next, to check the effect of URI deletion at adult stages, we genetically ablated URI in adult stages by maintaining *hURI1^(+/KI)*; *Pdx1^(tTA/+)*; *Uri1^{lox/lox}*; *Pdx1-cre* mice without doxycycline to activate hURI expression until 8 weeks of age. Then, mice were treated with doxycycline for 4 weeks to stop hURI induction. Notably, *hURI1^(+/KI)*; *Pdx1^(tTA/+)*; *Uri1^{lox/lox}*; *Pdx1-cre* mice with hURI repression did not show any signs of diabetes (Figures S2O and S2P). Thus, early URI ablation in the pancreas is deleterious for pre- and post-natal development, supporting the fact that URI loss in mice may lead to a MODY-like diabetes.

URI Controls *Pdx1* Methylation via ER α -Activating DNMT1

We next studied *Pdx1* promoter regulation by URI in cell lines *in vitro*. HEK293T cells were transiently transfected with different *Pdx1* promoter constructs fused to a gene encoding the enzyme chloramphenicol acetyltransferase (CAT).⁵⁰ Notably, HEK293T cells are readily transfectable and represent a more convenient model with high *PDX1* mRNA levels (Human Protein Atlas). The constructs contained the distal promoter, including the highly conserved AI, AII, and AIII regions homologous to human *PDX1* promoter regions PH1, PH2, and PH3⁵¹; the proximal promoter region to the transcription start site; and/or different 3' regions of the promoter (Figure S5A).⁵² All and AIII regions are known to contain regulatory sequences for β cell-specific lineage expression and function. HEK293T cells were then transfected with either siURI to deplete URI expression or pCDNA3-HA-

(H) Hematoxylin and eosin staining (H&E) of 7-week-old *Pdx1-cre* and *Uri1^{lox/lox}*; *Pdx1-cre* mice.

(I–K) β cell density (I), β cell mass (J), and average pancreatic islet size (K) of *Pdx1-cre* and *Uri1^{lox/lox}*; *Pdx1-cre* pancreatic islets (n = 8 and 5).

(L) Comparison and characteristics of diabetes in human and *Uri1^{lox/lox}*; *Pdx1-cre* mouse.

Data are means \pm SEMs. Statistical analysis done using Mantel-Cox test, Student's t test, and 2-way ANOVA. *p < 0.05; **p < 0.01; ***p < 0.001. Scale bar, 100 μ m in (H).

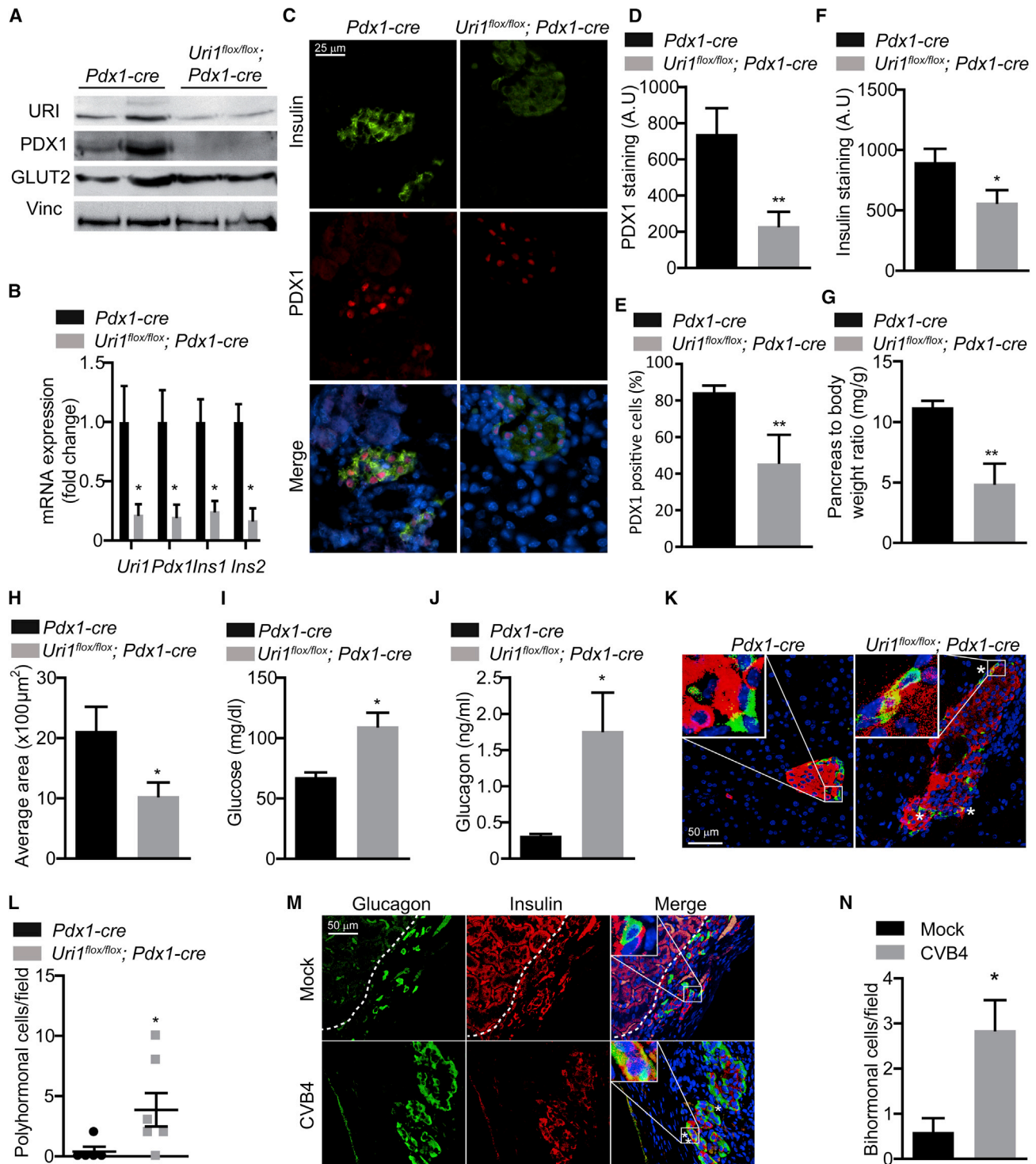


Figure 3. URI Controls PDX1 Expression and β Cell Identity in Mice

(A) WB of 7-week-old *Pdx1-cre* and *Uri1^{flox/flox}; Pdx1-cre* pancreases, normalized to GLUT2 expression. (B) qRT-PCR of indicated mRNA from 7-week-old *Pdx1-cre* and *Uri1^{flox/flox}; Pdx1-cre* pancreases, normalized to β-actin mRNA expression (n = 6 and 5). (C) IF of insulin and PDX1 in 2-day-old *Pdx1-cre* and *Uri1^{flox/flox}; Pdx1-cre* pancreases (post-natal). (D–F) Quantification of PDX1 nuclear expression (D), percentage of PDX1⁺ cells (E), and insulin expression (F) in 2-day-old *Pdx1-cre* and *Uri1^{flox/flox}; Pdx1-cre* pancreases (n = 6 and 7). (G) Pancreas to body weight of 2-day-old *Pdx1-cre* and *Uri1^{flox/flox}; Pdx1-cre* mice (n = 5).

(legend continued on next page)

URI to overexpress HA-URI (Figure S5B). Analysis of CAT activity 48 h post-transfection showed that URI downregulation significantly reduced *Pdx1* promoter activity, encompassing the regulatory elements AI–AIII, whereas URI overexpression increased it (Figures S5C and S5D). Thus, URI may regulate the core functions of pancreatic development and β cells through the *Pdx1* promoter.

Decreased PDX1 expression has been correlated with increased *Pdx1* promoter methylation in the glucose intrauterine growth retardation model in rats.⁵³ We therefore analyzed the methylation status of the *Pdx1* promoter at three sites containing the regulatory elements AI–AIII, supposedly regulated by URI. Bisulfite analysis and quantification of CpG-methylated sites in *Uri1^{flox/flox}; Pdx1-cre* pancreases indicated global methylation of the *Pdx1* promoter, with a most stringent increase in the regulatory element A2 (Figure 5A and S5E–S5H), suggesting that URI loss increases *Pdx1* methylation, possibly leading to its silencing in β cells and diabetes.

DNMT1, an S-adenosylmethionine-dependent DNA methyltransferase catalyzing DNA methylation, was recently proposed to maintain β cell identity; thus, its expression may be critical in the pathogenesis of diabetes, possibly through regulation of the *Pdx1* promoter.⁴³ *Pdx1* methylation is decreased in DNMT1 heterozygous mice.⁵⁴ Interestingly, in the pancreases of *Uri1^{flox/flox}; Pdx1-cre* mice, DNMT1 was significantly increased and specifically enriched in β cells, as shown by qRT-PCR and IHC (Figures 5B–5F). Notably, analyses of *Trdm1*, *Dnmt3a*, and *Dnmt3b* transcript levels indicated that there were no changes in the expression of other DNA methyltransferases in *Uri1^{flox/flox}; Pdx1-cre* pancreases (Figure S5I).

ER α is a well-known transcription factor that induces DNMT1 expression by binding to its promoter.⁵⁵ In addition, ER α reportedly forms an inactive cytoplasmic complex with URI and HSP90, and URI deletion promotes the nuclear translocation that ER α requires for transcriptional activity.²⁹ We detected endogenous interaction between URI and ER α in INS-1E cells, MCF-7 breast cancer cells (known to have high levels of ER α)⁵⁶ and *Pdx1-cre* pancreases in co-immunoprecipitation (coIP) experiments, but not in *Uri1^{flox/flox}; Pdx1-cre* pancreases (Figures 5G, S5J, and S5K), indicating its specificity. As mentioned, translocation to the nucleus is required for the transcriptional activity of ER α , and URI has been shown to sequester it in the cytoplasm.²⁹ By subcellular fractionation of INS-1E cells, we confirmed that URI knockdown induced ER α nuclear translocation and PDX1 downregulation (Figure 5H). We then verified that ER α directly activates *Dnmt1* expression, by chromatin immunoprecipitation (ChIP) assays, and showed that ER α bound to *Dnmt1* promoter regions containing two ER elements (EREs) (Figures 5I and S5L).⁵⁷ Notably, URI could not be found to bind

Pdx1 promoter (Figure S5M). Therefore, URI binds and sequesters ER α in the cytoplasm, thereby abolishing the transcription of DNMT1. URI loss increases DNMT1 expression and *Pdx1* promoter methylation.

Procainamide-Mediated DNMT1 Inhibition Reinstates PDX1 Expression and Glucose Tolerance by Reducing Hypermethylation of *Pdx1* Promoter in Mice

Prompted by these observations, we treated *Uri1^{flox/flox}; Pdx1-cre* mice since conception with the demethylating agent procainamide, a highly specific non-nucleoside inhibitor of DNMT1.⁵⁸ Procainamide-treated *Uri1^{flox/flox}; Pdx1-cre* mice showed better glucose clearance than non-treated *Uri1^{flox/flox}; Pdx1-cre* mice (Figure 6A). Furthermore, we detected no aberrations in their insulin tolerance (Figure S6A). IF, WB, and qRT-PCR analyses showed that the lost PDX1 expression was reinstated in pancreatic islets of procainamide-treated *Pdx1-cre* and *Uri1^{flox/flox}; Pdx1-cre* mice (Figures 6B–6F). *Pdx1* promoter hypermethylation was reversed in procainamide-treated *Uri1^{flox/flox}; Pdx1-cre* mice when compared to non-treated *Uri1^{flox/flox}; Pdx1-cre* mice (Figures 6G, S6B, and S6C). Interestingly, pancreatic PDX1 and URI were substantially increased in procainamide-treated *Pdx1-cre* mice, and the expression patterns were similar (Figure 6E), suggesting homeostatic methylation of *Uri1* promoter to balance URI expression. In line with these findings, insulin content in procainamide-treated *Uri1^{flox/flox}; Pdx1-cre* was slightly lower (but not significant) when compared to procainamide-treated *Pdx1-cre* mice (Figure S6D), most likely due to differences in URI expression in procainamide-treated mice (Figure 6E). Notably, pancreatic AhR expression was not altered in procainamide-treated mice when compared to non-treated mice (Figure S6E).

Finally, the analysis of CVB4-infected human grafts showed a significant increase in the number of DNMT1⁺ cells, inversely correlating with URI loss (Figures 6H and 6I). Thus, URI loss activates ER α -mediated DNMT1 expression in pancreases, possibly by promoting *Pdx1* promoter methylation and silencing, and diabetes.

URI and PDX1 Expression Correlates in Diabetic Mice

PDX1 is known to be downregulated in mouse pancreases by nutrient-induced stress factors, such as a high-fat diet (HFD),⁵⁹ further highlighting the possible contribution of nutrient overload in diabetes pathogenesis. We therefore treated C57BL/6J mice with HFD for 32 weeks and found, concomitant to PDX1 and insulin downregulation, a significant decrease in URI expression in the endocrine compartment (Figures S7A and S7B). PDX1 loss may also putatively account for β cell failure in HFD-induced T2D.⁶⁰ Accordingly, HFD-treated *hURI1^(+/K); Pdx1^(TTA/+)* mice

(H) Area of pancreatic islets per field in 2-day-old *Pdx1-cre* and *Uri1^{flox/flox}; Pdx1-cre* pancreases (n = 6 and 7).

(I) Fasting glucose levels of 2-day-old *Pdx1-cre* and *Uri1^{flox/flox}; Pdx1-cre* mice (n = 7 and 8).

(J) Fasting glucagon levels of 7-week-old *Pdx1-cre* and *Uri1^{flox/flox}; Pdx1-cre* mice (n = 12 and 11).

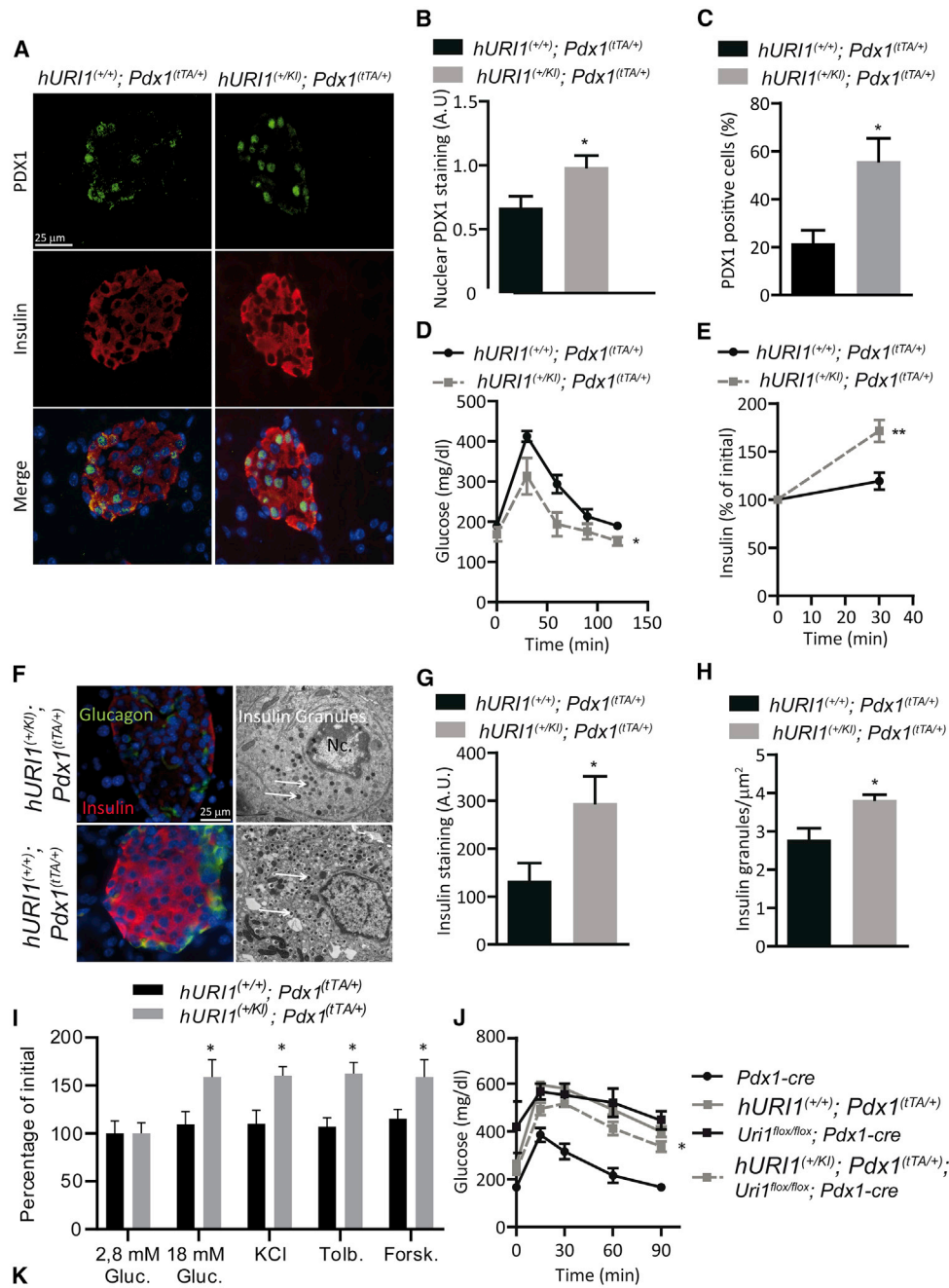
(K) Confocal IF of insulin (red) and glucagon (green) in 7-week-old *Pdx1-cre* and *Uri1^{flox/flox}; Pdx1-cre* pancreases.

(L) Quantification of polyhormonal cells per field in 7-week-old *Pdx1-cre* and *Uri1^{flox/flox}; Pdx1-cre* pancreases. Up to 5 fields in 1 cut per sample were examined (n = 5 and 6).

(M) Confocal IF of insulin and glucagon from CVB4-infected human pancreas xenografts in mice. Asterisks represent bihormonal cells.

(N) Quantification of bihormonal—insulin and glucagon—positive cells. Up to 5 fields in 1 cut per sample were examined (n = 10 and 7).

Data are means \pm SEMs. Statistical analysis done using Student's t test. *p < 0.05; **p < 0.01. Scale bar, 25 μ m in (C) and 50 μ m in (K) and (M).



	<i>hURI1^(+/+); Pdx1^(TTA/+); Uri1^{fllox/fllox}; Pdx1-cre</i>	<i>hURI1^(+/KI); Pdx1^(TTA/+); Uri1^{fllox/fllox}; Pdx1-cre</i>
Probability	0.059	0.057
number of pups	136	117
number of expected mice	8.0268	6.6875
number of borned mice	0	6

(legend on next page)

presented better glucose tolerance with no apparent alteration in insulin sensitivity (Figures S7C and S7D). In addition, crosses of $hURI1^{(+/KJ)}$; $Pdx1^{(T/A/+)}$ and heterozygous leptin-deficient mice ($ob/+$) ($ob/+$; $hURI1^{(+/KJ)}$; $Pdx1^{(T/A/+)}$ mice) had better glucose tolerance, resembling $hURI1^{(+/+)}$; $Pdx1^{(T/A/+)}$ mice, than glucose-intolerant $ob/+$ mice ($ob/+$; $hURI1^{(+/KJ)}$; $Pdx1^{(T/A/+)}$) (Figures S7E and S7F). These findings suggest that URI overexpression protects from nutrient overload-induced diabetes (possibly mediated by PDX1 loss). They also suggest a general mechanism involving the activation of *Pdx1* promoter methylation and silencing in response to various exogenous stimuli implicated in the pathogenesis of diabetes in humans.

Coxsackieviruses and URI, DNMT1, and PDX1 Expression Correlate in Human Diabetic and Non-diabetic Patients

Next, to investigate the clinical relevance of our findings, we analyzed coxsackievirus VP1 and URI, insulin, PDX1, and DNMT1 levels in pancreases from non-diabetic ($n = 54$), T2D ($n = 19$), and T1D ($n = 6$) patients. T2D patients suffer from compensative β cell expansion, hyperinsulinemia, and β cell failure in an insulin resistance state,⁶¹ whereas the loss of β cell identity is found in T1D patients.^{43,46} In this context, β cell density was not changed in diabetic samples when compared to non-diabetic samples, but β cell mass was decreased (Figures S7G and S7H). Notably, IF analysis showed that URI and insulin expression in the islets was decreased in T2D and T1D human samples (Figures 7A–7C and S7I). URI positively correlated with insulin levels (Figure 7D). Moreover, analysis of PDX1 and DNMT1 expression in the islets by IHC indicated that percentage of PDX1⁺ cells decreased in T2D and T1D patients when compared to the non-diabetic samples, whereas DNMT1⁺ cells significantly increased (Figures 7E–7G). Strikingly, URI and PDX1 expressions positively correlated (Figures 7H and S7J).

Next, we investigated the presence of VP1 in T2D and T1D samples since coxsackievirus infection correlates with a higher risk of T1D incidence,^{11,62} and VP1 has been detected in some pancreatic islets of T2D patients and all samples of a cohort of patients with recent onset of T1D.^{14,63} An IHC analysis of VP1 staining revealed 83% positive samples (5 of 6) in the endocrine pancreas of T1D patients and 23% positive samples (5 of 22) in T2D samples, in contrast to only 5% positive samples (3 of 57) in non-diabetic samples (Figure 7I). Finally, we analyzed the percentage of PDX1⁺ and DNMT1⁺ cells and we scored for URI

expression in endocrine pancreases from VP1⁺ samples. PDX1, DNMT1, and URI expression correlated with the infection status (Figures 7J–7L), corroborating results shown in β cell lines and in human grafts. These data suggest a strong correlation between CVB4 infection, URI loss, DNMT1 expression, and PDX1 silencing, thereby causing diabetes.

DISCUSSION

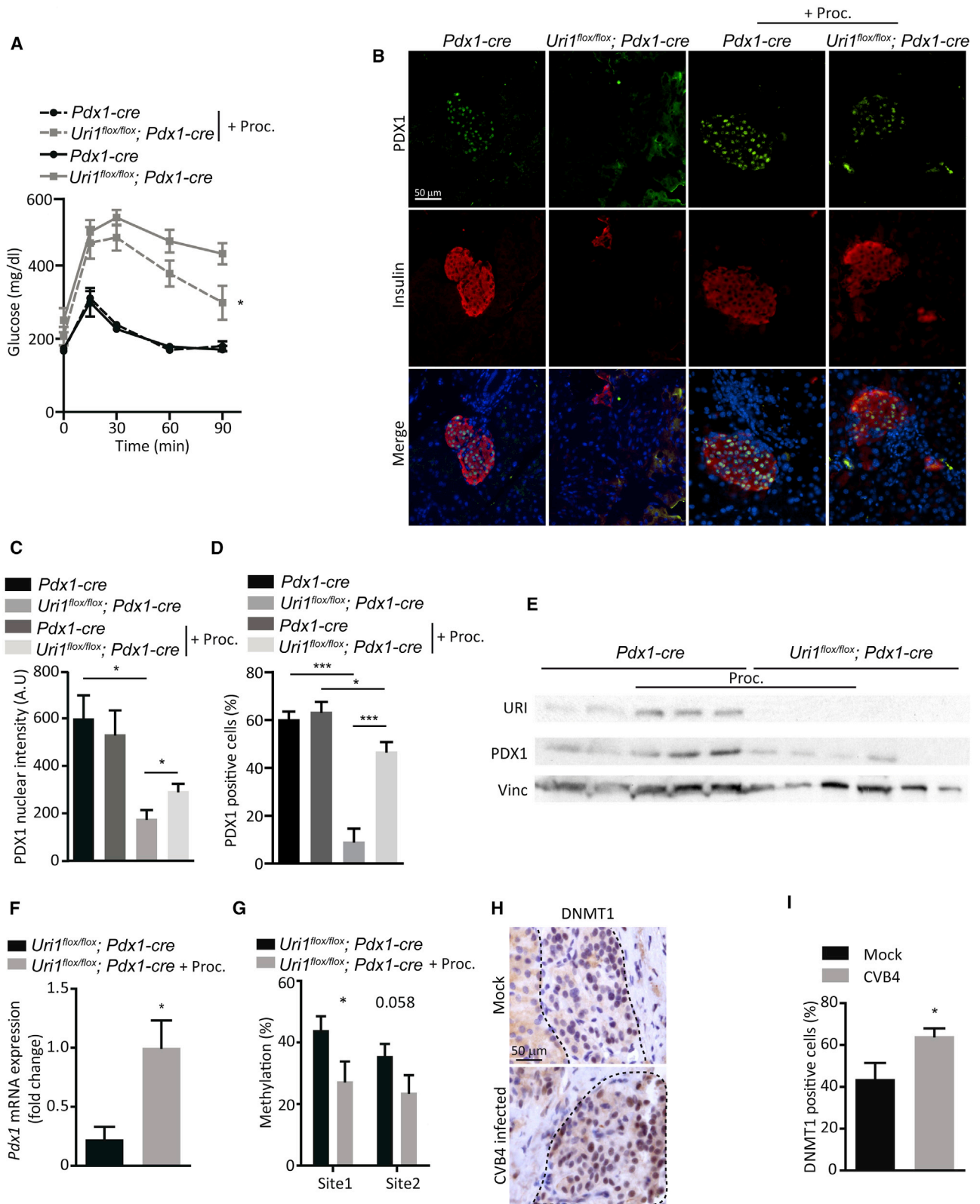
The dense networks of interactions between environmental stressors and biological systems pose major challenges in efforts to elucidate the underlying mechanisms of diabetes and obtain the holistic understanding required for robust prevention and treatment. Responses to environmental factors through the regulation and expression of proteins that have important protective functions, but are potentially damaging if inappropriately expressed, may play frequently underestimated roles in various pathological states. Here, we provide mechanisms governing the relationship between enterovirus infection and the development of diabetes. We show that CVB4 infection causes URI loss in β cells, leading to DNMT1 expression and PDX1 silencing, and subsequently inducing β cell loss and hyperglycemia. Thus, URI and DNMT1 expressions and PDX1 silencing causally link enterovirus infection to diabetes.

Although enterovirus infection has been mainly linked to T1D, our present work supports that CVB4 infection can induce a loss of β cell identity, leading to hyperglycemia in the absence of autoimmunity. This loss of PDX1 suggests a MODY-like diabetes, reminiscent of MODY4, caused by loss-of-function mutations in PDX1,¹⁷ rather than T1D. This is also supported by the fact that the phenotype observed in *Uri1^{fllox/fllox}*; *Pdx1-cre* mice is strongly dependent on the restoration of PDX1 expression. Moreover, that early URI ablation in the pancreas is deleterious to pre- and post-natal development supports the evidence that URI loss in mice may lead to a MODY-like diabetes, although an idiopathic T1D subtype cannot be excluded.

T1D has long been considered a genetic autoimmune disease in which T cell infiltration induces the destruction of insulin-producing β cells of pancreatic islets. However, more recent data implicate environmental assaults as premises of β cell dysfunction and T1D onset.²⁰ In this context, viral-mediated β cell identity loss and transdifferentiation are novel, but also controversial lines of investigation.⁴⁸ In fact, T1D is related to the presence of islet cells dually expressing insulin and glucagon; likewise,

Figure 4. URI Is Required to Maintain Glucose Homeostasis by Regulating PDX1 Expression

(A) IF of PDX1 and insulin in 7-week-old $hURI1^{(+/KJ)}$; $Pdx1^{(T/A/+)}$ and $hURI1^{(+/+)}$; $Pdx1^{(T/A/+)}$ pancreases.
 (B and C) Quantification of PDX1 nuclear expression (B) and percentage of PDX1⁺ cells (C) in 7-week-old $hURI1^{(+/KJ)}$; $Pdx1^{(T/A/+)}$ and $hURI1^{(+/+)}$; $Pdx1^{(T/A/+)}$ pancreases ($n = 8$ and 7).
 (D and E) Glucose tolerance (D) and insulin secretion tests (E) in 7-week-old $hURI1^{(+/KJ)}$; $Pdx1^{(T/A/+)}$ and $hURI1^{(+/+)}$; $Pdx1^{(T/A/+)}$ females ($n = 7$ and 6).
 (F) IF of insulin and glucagon and transmission electron microscopy in 7-week-old $hURI1^{(+/KJ)}$; $Pdx1^{(T/A/+)}$ and $hURI1^{(+/+)}$; $Pdx1^{(T/A/+)}$ pancreases.
 (G) Quantification of insulin in 7-week-old $hURI1^{(+/KJ)}$; $Pdx1^{(T/A/+)}$ and $hURI1^{(+/+)}$; $Pdx1^{(T/A/+)}$ pancreases ($n = 5$).
 (H) Quantification of insulin granules in 7-week-old $hURI1^{(+/KJ)}$; $Pdx1^{(T/A/+)}$ and $hURI1^{(+/+)}$; $Pdx1^{(T/A/+)}$ pancreases ($n = 4$).
 (I) Insulin secretion in isolated islets of 7-week-old $hURI1^{(+/+)}$; $Pdx1^{(T/A/+)}$ and $hURI1^{(+/KJ)}$; $Pdx1^{(T/A/+)}$ pancreases stimulated for 30 min with either 2.6 nM glucose, 18 nM glucose, 20 mM KCl, 100 μ M tolbutamide, or 1 μ M forskolin ($n = 12$ and 11).
 (J) Glucose tolerance test in 7-week-old *Pdx1-cre*, $hURI1^{(+/+)}$; $Pdx1^{(T/A/+)}$, *Uri1^{fllox/fllox}*; *Pdx1-cre*, and $hURI1^{(+/KJ)}$; $Pdx1^{(T/A/+)}$; *Uri1^{fllox/fllox}*; *Pdx1-cre* females ($n = 5$, 8, 10). Statistical analysis done between $hURI1^{(+/+)}$; $Pdx1^{(T/A/+)}$ and $hURI1^{(+/KJ)}$; $Pdx1^{(T/A/+)}$; *Uri1^{fllox/fllox}*; *Pdx1-cre*.
 (K) Statistical differences in natality of $hURI1^{(+/+)}$; $Pdx1^{(T/A/+)}$; *Uri1^{fllox/fllox}*; *Pdx1-cre* and $hURI1^{(+/KJ)}$; $Pdx1^{(T/A/+)}$; *Uri1^{fllox/fllox}*; *Pdx1-cre* mice.
 Data are means \pm SEMs. Statistical analysis done using Student's t test and 2-way ANOVA. * $p < 0.05$; ** $p < 0.01$. Scale bar, 2 μ m in (F) and 25 μ m in (A) and (F).



(legend on next page)

this regard, we have shown that CVB4 in a dose-dependent manner causes the loss of URI without provoking any cytotoxic effects or cell death, even at high doses of CVB4. Finally, the CVB4 sequence generated by Dotta et al. shared >99% nucleotide identity with the CVB4 strain sequenced by Sickles et al. in 1951, raising questions on the CVB4 origin from Dotta et al.^{9,70,71} Therefore, environmental factors may drive the development of an idiopathic T1D, but the immune components, as a secondary response, could contribute to β cell failure.

This observation is also supported by our work conducted using human samples that shows that long-term β cell alteration due to viral infection may participate in the onset of both T1D and T2D, although an idiopathic T1D subtype could not be excluded either. It is indeed relevant to observe that the incidence of VP1 detection may be greater in T1D than in T2D patients. It is thus tempting to speculate that CVB4 can lead to heterogenic, and in some cases, fulminant autoimmune responses in T1D that could obviate URI-mediated PDX1 downregulation and β cell identity loss. Alterations in *Pdx1* methylation status may also be induced by a broader spectrum of factors that can impair glucose homeostasis, such as nutrient overload,⁵⁹ corroborating its importance to the maintenance of proper β cell function during various environmental assaults. Although lineage tracing experiments would be needed to demonstrate cellular plasticity in diabetes in *Uri1^{fllox/fllox}; Pdx1-cre* mice, our data suggest that the conversion of β cells into α cells may contribute to the loss of β cells,^{46,72} and the reprogramming of α cells into insulin-producing cells may be an adaptive mechanism that compensates for the destruction of β cells during diabetes pathogenesis.

Finding the ideal model in mice for the study of β cell homeostasis remains challenging. The *Pdx1*-driven transgenic mouse model is a useful tool to study the endocrine pancreas, but it also may target other PDX1-expressing cells, including the duodenum. Although hyperglycemia has been shown to induce intestinal barrier dysfunction, dysbiosis, and enhanced abdominal cavity in a model of streptozotocin (STZ) administration,⁷³ we did not observe defects in intestinal structure and permeability. Notably, the specific deletion of PDX1 in intestinal epithelial cells did not lead to a specific phenotype, related to neither glucose homeostasis nor epithelial barrier disruption.⁷⁴ Therefore, alterations in the intestinal epithelium may not be the cause of glucose intolerance or the increased morbidity in the *Uri1^{fllox/fllox}; Pdx1-cre* mice. The cause of *Uri1^{fllox/fllox}; Pdx1-cre* mouse death may be related to hyperglycemia, as mice collected at a humane endpoint were displaying blood glucose levels >500 mg/dL (data not shown).

Uri1^{fllox/fllox}; Pdx1-cre mice showed increased glucose intolerance and higher mortality in males. Female mice are more insulin sensitive when compared to males, and glucose levels settled back to normoglycemia after 60 min in females, whereas males were still hyperglycemic (Figures 2E and S2H). Since the cytoplasmic ER maintains β cell survival and glucose homeostasis and ER gene polymorphism affects the age of onset of T1D,^{30,32} it is tempting to speculate that estrogen levels may provide protective effects in diabetes. Interestingly, URI binds and inhibits ER, limiting the estrogen effects. Knowing that males have less estrogen than females, the ER inhibition by URI may be more pronounced in males, explaining the gender differences observed in *Uri1^{fllox/fllox}; Pdx1-cre* mice.

We also note that β cell reprogramming to alternative islet cell fates may putatively account for β cell failure in obesity-induced diabetes.^{3,75–77} As URI is downregulated following nutrient surpluses, potentially leading to diabetes, and it is a molecular chaperone that responds to various environmental stressors, its loss may be a key pathogenic trigger of diabetes and feature of the “environmental/pathogen paradigm” of disease. How URI expression is regulated by various environmental stressors remains an open question. CVB4 and nutrient overload can be inflammatory, and hence, inflammatory cues may modulate URI expression in the pancreas.

Finally, since severe acute respiratory virus-coronavirus-2 (SARS-CoV-2) may trigger diabetes by damaging β cells independently of the immune response,^{78–80} it would be interesting to check whether SARS-CoV-2 downregulates URI in β cells and induces PDX1 silencing and hence the development of “new-onset diabetes.”⁷⁹

The identification of URI and DNMT1 expression and PDX1 silencing as likely causal links between environmental stresses and diabetes may facilitate the development of innovative new avenues and mechanism-based therapeutics to counter the disease. Targeting hypermethylation of the *Pdx1* promoter using DNA methyltransferase inhibitors with antiviral therapies may therefore be future elegant preventive strategies for patients at high risk of developing diabetes. Notably, despite their limitations as to their off-target effects and efficient delivery, several DNA demethylases are licensed for clinical use in cancer therapy, which should aid the development of such strategies.

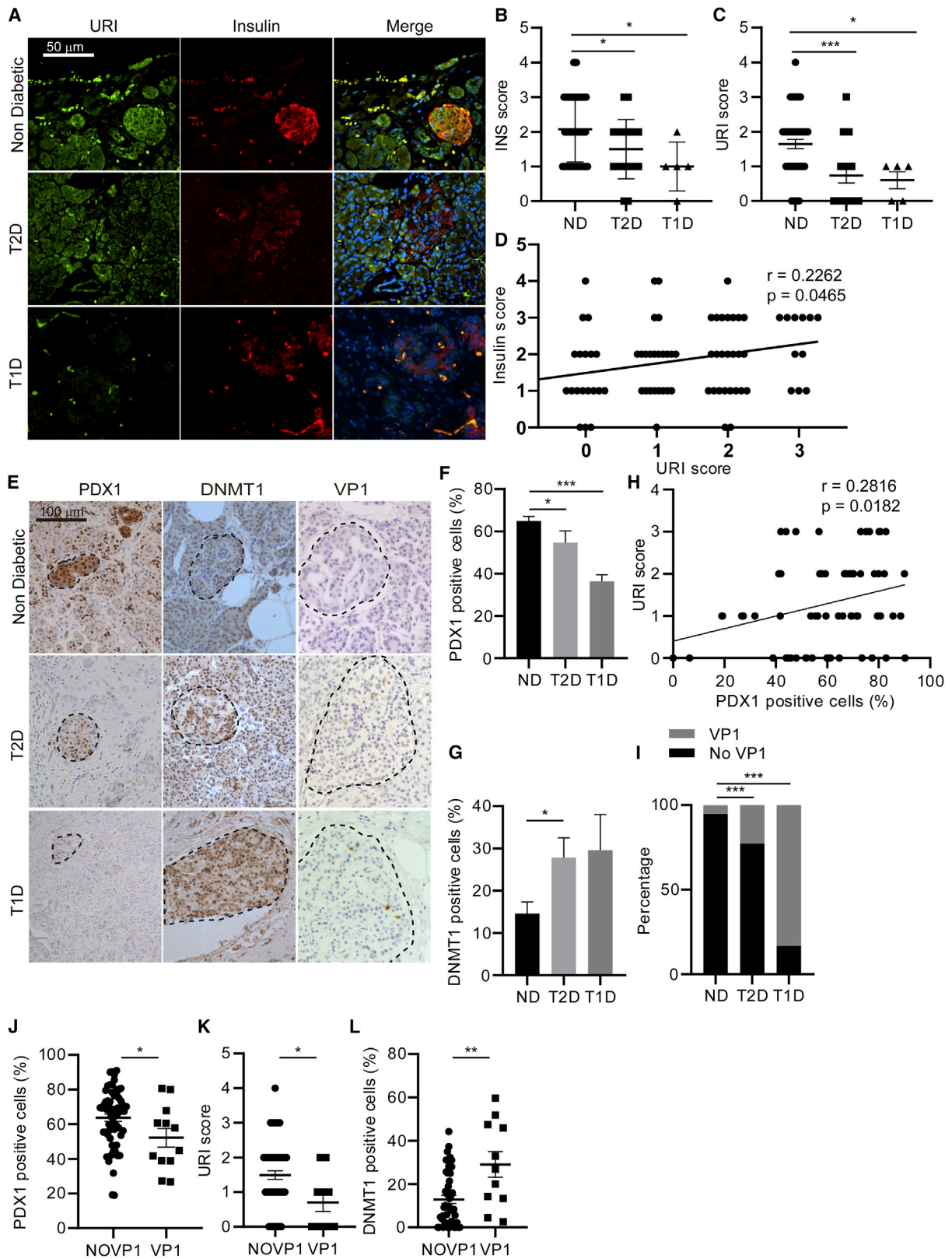
Limitations of Study

We acknowledge that the mechanism described in this article may represent one of many disease endotypes that are most likely related to an idiopathic T1D or MODY-like diabetes—

Figure 6. Procainamide-Mediated DNMT1 Inhibition Reinstates PDX1 Expression and Glucose Tolerance by Reducing Hypermethylation of *Pdx1* Promoter in Mice

- (A) Glucose tolerance test in *Pdx1-cre* and *Uri1^{fllox/fllox}; Pdx1-cre* males treated or not treated with procainamide (n = 6 and 5).
 (B) IF of 7-week-old *Pdx1-cre* and *Uri1^{fllox/fllox}; Pdx1-cre* pancreases treated or not treated with procainamide and stained for insulin and PDX1.
 (C and D) Quantification of nuclear PDX1 expression (C) and percentage of positive cells (D) in 7-week-old *Pdx1-cre* and *Uri1^{fllox/fllox}; Pdx1-cre* pancreases treated or not treated with procainamide (n = 5, 6, 6, and 7).
 (E) WB of URI, PDX1, and vinculin in 7-week-old *Pdx1-cre* and *Uri1^{fllox/fllox}; Pdx1-cre* pancreases treated or not treated with procainamide.
 (F) qRT-PCR of *Pdx1* in *Uri1^{fllox/fllox}; Pdx1-cre* males treated or not treated with procainamide (n = 6).
 (G) Percentage of methylation in 2 different sites of *Pdx1* promoter in *Uri1^{fllox/fllox}; Pdx1-cre* males treated or not treated with procainamide (n = 5 and 4).
 (H) IHC of DNMT1 in CVB4-infected human pancreas xenografts in mice. Dashed lines denote endocrine compartment.
 (I) Quantification of DNMT1⁺ cells (n = 5 and 6).

Data are means \pm SEMs. Statistical analysis done using Student's t test and 2-way ANOVA. *p < 0.05. Scale bar, 50 μ m in (B) and (H).



(legend on next page)

possibly to MODY4—and further validation in human tissues would be required. In particular, we did not attempt to infect mice with CVB4 and assess for URI, DNMT1, and PDX1 expression and the development of diabetes. In addition, the CVB4 infection of live pancreas slices from human organ donors⁶⁹ would have validated our mechanistic data and would have been a proof-of-concept study *in vivo*, linking functional data to intact human tissues. We used the Pdx1-Cre line to genetically ablate URI in pancreata, although the Rip-Cre line could have also been tested. However, neither the Pdx1-Cre line nor the Rip-Cre line deletes specifically in β cells, and both lines may present advantages and disadvantages. Rip-Cre line has strong unspecific effects in the hypothalamus. Experimental evidence suggests that Rip-Cre mice display glucose intolerance.⁸¹ The Ins1-CreERT2 line could have been an alternative, particularly to deplete URI in the adult stage. Furthermore, mouse lineage tracing experiments would have supported the transdifferentiation of β cells into α cells. Finally, a population-based epidemiological study with cancer patients treated with DNA methyltransferase inhibitors could demonstrate their potential clinical benefits for diabetes.

STAR★METHODS

Detailed methods are provided in the online version of this paper and include the following:

- KEY RESOURCES TABLE
- RESOURCE AVAILABILITY
 - Lead Contact
 - Materials Availability
 - Data and Code Availability
- EXPERIMENTAL MODEL AND SUBJECT DETAILS
 - Mouse Models
 - CVB4-Infected Mice Grafted with Human Islets
 - Human Islets for the Experiments *In Vitro*
 - Human Pancreatic Samples
 - Cell Lines
- METHOD DETAILS
 - Mouse Handling
 - Mouse Diets and Treatments
 - Isolation of Mouse Pancreatic Islets

- Insulin Secretion Test (IST) in Isolated Islets
- Glucose Tolerance Test (GTT) in Mice
- Insulin Tolerance Test (ITT) in Mice
- Insulin Secretion Test (IST) in Mice
- Plasmid Transfection and siRNA Experiments
- CVB4 Infections in Cells
- CVB4 Infection of Human Islets
- Flow Cytometry
- Pancreatic Insulin Content
- Blood Parameters
- FITC-Dextran Assay
- Immunoprecipitation
- Chromatin Immunoprecipitation
- Cell Fractionation
- CAT Assay
- Immunoblotting
- Immunohistochemistry
- Immunofluorescence
- Electron Microscopy
- Bisulfite Sequencing
- Genotyping
- qRT-PCR
- QUANTIFICATION AND STATISTICAL ANALYSIS
 - Statistical Analysis
 - Image Analysis
 - Scoring Signal in Human Samples
 - β cell Mass Quantification

SUPPLEMENTAL INFORMATION

Supplemental Information can be found online at <https://doi.org/10.1016/j.xcrm.2020.100125>.

ACKNOWLEDGMENTS

Human diabetic pancreatic samples and data were obtained from the CNIO Biobank thanks to the help of Maria-Jesus Artiga and from Biobanc-Mur, Mar-Biobank, Vasque Biobank, and Andalusian Public Health System Biobank, integrated in the Spanish Biobank Network and funded by Instituto de Salud Carlos III. We are also thankful to the Biobank of IDIBAPS, Barcelona, for providing samples to A.N. Samples were processed following standard operating procedures with the appropriate approval of the Ethics and Scientific Committees. We also thank the CNIO Mouse Genome Editing Core Unit as well as the CNIO Genomics Unit for their support. We are also thankful to

Figure 7. Coxsackieviruses and URI, DNMT1, and PDX1 Expression Correlates in Human Diabetic Patients

(A) IF of URI and insulin in human pancreases of non-diabetic (ND), type 1 diabetes (T1D), and type 2 diabetes (T2D) samples. Representative images from individual donors are shown.

(B) Insulin scoring in human pancreases of ND, T1D, and T2D samples (n = 52, 19, and 6, respectively). 0 = absent, 1 = minimal, 2 = mild, 3 = marked, 4 = strong.

(C) URI scoring in human pancreases of ND, T1D, and T2D samples (n = 54, 19, and 6). 0 = absent, 1 = minimal, 2 = mild, 3 = marked, 4 = strong.

(D) Pearson correlation between insulin score and URI score in human pancreatic islets of ND, T1D, and T2D samples (n = 74).

(E) IHC of PDX1, DNMT1, and VP1 in human pancreases of ND, T1D, and T2D samples. A pathologist confirmed that VP1⁺ cells are in endocrine cells. Black dotted lines represent pancreatic islets. Representative images from individual donors are shown.

(F) Quantification of PDX1⁺ cells in human pancreases of ND, T1D, and T2D samples (n = 54, 19, and 6).

(G) Quantification of DNMT1⁺ cells in human pancreases of ND, T1D, and T2D samples. (n = 54, 19, and 5).

(H) Pearson correlation between PDX1⁺ cells and URI score in human pancreases of ND, T1D, and T2D samples (n = 68).

(I) Percentage of samples with either no VP1 (NO VP1) or VP1 in human pancreases of ND, T1D, and T2D samples (n = 60, 23, and 6, respectively).

(J) Percentage of PDX1⁺ cells in human sample VP-1⁺ (VP1) or VP1⁻ (NO VP1) in the endocrine pancreases of non-diabetic and diabetic samples (n = 63 and 12).

(K) URI score in human sample VP-1⁺ (VP1) or VP1⁻ (NO VP1) in the endocrine pancreas (n = 67 and 10).

(L) Percentage of DNMT1⁺ cells in human samples that are VP1⁺ (VP1) or VP1⁻ (NO VP1) in the endocrine pancreas (n = 47 and 11).

Data are means \pm SEMs. Statistical analysis done using Student's t test, Mann-Whitney test, chi-square test, and Pearson correlation. *p < 0.05; **p < 0.01; ***p < 0.001. Scale bar, 50 μ m in (A) and 100 μ m in (E).

Dr. K. Qvortrup (University of Copenhagen, Denmark) for the electron microscopy. This work was funded by grant to J.P.W. supported by the National Institutes of Health NIAID/NIDDK R01 AI116920, and by grants to N.D. supported by the EFSD/JRDF/Lilly Programme through the European Foundation for the Study of Diabetes (EFSD) and and by the State Research Agency (AEI, 10.13039/501100011033) from the Spanish Ministry of Science and Innovation (projects SAF2016-76598-R, SAF2017-92733-EXP, and RTI2018-094834-B-I00) through the European Regional Development Fund (ERDF). This work was developed at the CNIO, which is funded by the Health Institute Carlos III (ISCIII) and the Spanish Ministry of Science and Innovation.

AUTHOR CONTRIBUTIONS

H.B. designed, performed, and analyzed most of the experiments. A.T. contributed, performed, and analyzed most of the experiments in the URI loss-of-function mice. A.C.-P. performed the immunoprecipitation assays. C.P. analyzed the histology of mouse and human tissues. B.S. and J.P.W. kindly provided the CVB4-infected human pancreatic samples. A.N. provided some human pancreatic samples. J.P.W. participated in fruitful discussions and helped in correcting the manuscript. N.D. designed the experiments, analyzed the data, conceived the project, and wrote the manuscript. The funding was secured by N.D.

DECLARATION OF INTERESTS

The authors declare no competing interests.

Received: June 29, 2018

Revised: August 6, 2020

Accepted: September 22, 2020

Published: October 20, 2020

REFERENCES

- Ilonen, J., Lempainen, J., and Veijola, R. (2019). The heterogeneous pathogenesis of type 1 diabetes mellitus. *Nat. Rev. Endocrinol.* *15*, 635–650.
- Soleimanpour, S.A., and Stoffers, D.A. (2013). The pancreatic β cell and type 1 diabetes: innocent bystander or active participant? *Trends Endocrinol. Metab.* *24*, 324–331.
- Talchai, C., Xuan, S., Lin, H.V., Sussel, L., and Accili, D. (2012). Pancreatic β cell dedifferentiation as a mechanism of diabetic β cell failure. *Cell* *150*, 1223–1234.
- Imagawa, A., Hanafusa, T., Miyagawa, J., and Matsuzawa, Y.; Osaka IDDM Study Group (2000). A novel subtype of type 1 diabetes mellitus characterized by a rapid onset and an absence of diabetes-related antibodies. *N. Engl. J. Med.* *342*, 301–307.
- Guarnotta, V., Vigneri, E., Pillitteri, G., Ciresi, A., Pizzolanti, G., and Giordano, C. (2018). Higher cardiometabolic risk in idiopathic versus autoimmune type 1 diabetes: a retrospective analysis. *Diabetol. Metab. Syndr.* *10*, 40.
- Piñero-Piloña, A., and Raskin, P. (2001). Idiopathic type 1 diabetes. *J. Diabetes Complications* *15*, 328–335.
- Wilkin, T.J. (2012). The convergence of type 1 and type 2 diabetes in childhood: the accelerator hypothesis. *Pediatr. Diabetes* *13*, 334–339.
- Yoon, J.W., Austin, M., Onodera, T., and Notkins, A.L. (1979). Isolation of a virus from the pancreas of a child with diabetic ketoacidosis. *N. Engl. J. Med.* *300*, 1173–1179.
- Dotta, F., Censini, S., van Halteren, A.G., Marselli, L., Masini, M., Dionisi, S., Mosca, F., Boggi, U., Muda, A.O., Del Prato, S., et al. (2007). Coxsackie B4 virus infection of beta cells and natural killer cell insulinitis in recent-onset type 1 diabetic patients. *Proc. Natl. Acad. Sci. USA* *104*, 5115–5120.
- Harley, J.B., Chen, X., Pujato, M., Miller, D., Maddox, A., Forney, C., Magnusen, A.F., Lynch, A., Chetal, K., Yukawa, M., et al. (2018). Transcription factors operate across disease loci, with EBNA2 implicated in autoimmunity. *Nat. Genet.* *50*, 699–707.
- Gallagher, G.R., Brehm, M.A., Finberg, R.W., Barton, B.A., Shultz, L.D., Greiner, D.L., Bortell, R., and Wang, J.P. (2015). Viral infection of engrafted human islets leads to diabetes. *Diabetes* *64*, 1358–1369.
- Knip, M. (2011). Pathogenesis of type 1 diabetes: implications for incidence trends. *Horm. Res. Paediatr.* *76 (Suppl 1)*, 57–64.
- Kracht, M.J.L., van Lummel, M., Nikolic, T., Joosten, A.M., Laban, S., van der Slik, A.R., van Veelen, P.A., Carlotti, F., de Koning, E.J., Hoeben, R.C., et al. (2017). Autoimmunity against a defective ribosomal insulin gene product in type 1 diabetes. *Nat. Med.* *23*, 501–507.
- Krogvold, L., Edwin, B., Buanes, T., Frisk, G., Skog, O., Anagandula, M., Korsgren, O., Undlien, D., Eike, M.C., Richardson, S.J., et al. (2015). Detection of a low-grade enteroviral infection in the islets of langerhans of living patients newly diagnosed with type 1 diabetes. *Diabetes* *64*, 1682–1687.
- Dunne, J.L., Richardson, S.J., Atkinson, M.A., Craig, M.E., Dahl-Jørgensen, K., Flodström-Tullberg, M., Hyöty, H., Insel, R.A., Lernmark, Å., Lloyd, R.E., et al. (2019). Rationale for enteroviral vaccination and antiviral therapies in human type 1 diabetes. *Diabetologia* *62*, 744–753.
- Ahlgren, U., Jonsson, J., Jonsson, L., Simu, K., and Edlund, H. (1998). Beta-cell-specific inactivation of the mouse *Ipf1/Pdx1* gene results in loss of the beta-cell phenotype and maturity onset diabetes. *Genes Dev.* *12*, 1763–1768.
- Melloul, D., Marshak, S., and Cerasi, E. (2002). Regulation of *pdx-1* gene expression. *Diabetes* *51 (Suppl 3)*, S320–S325.
- Gao, T., McKenna, B., Li, C., Reichert, M., Nguyen, J., Singh, T., Yang, C., Pannikar, A., Doliba, N., Zhang, T., et al. (2014). *Pdx1* maintains β cell identity and function by repressing an α cell program. *Cell Metab.* *19*, 259–271.
- Glavas, M.M., Hui, Q., Tudurí, E., Erener, S., Kasteel, N.L., Johnson, J.D., and Kieffer, T.J. (2019). Early overnutrition reduces *Pdx1* expression and induces β cell failure in Swiss Webster mice. *Sci. Rep.* *9*, 3619.
- Evans-Molina, C., Sims, E.K., DiMeglio, L.A., Ismail, H.M., Steck, A.K., Palmer, J.P., Krischer, J.P., Geyer, S., Xu, P., and Sosenko, J.M.; Type 1 Diabetes TrialNet Study Group (2018). β Cell dysfunction exists more than 5 years before type 1 diabetes diagnosis. *JCI Insight* *3*, 3.
- Sane, F., Caloone, D., Gmyr, V., Engelmann, I., Belaich, S., Kerr-Conte, J., Pattou, F., Desailoud, R., and Hober, D. (2013). Coxsackievirus B4 can infect human pancreas ductal cells and persist in ductal-like cell cultures which results in inhibition of *Pdx1* expression and disturbed formation of islet-like cell aggregates. *Cell. Mol. Life Sci.* *70*, 4169–4180.
- Nyalwidhe, J.O., Gallagher, G.R., Glenn, L.M., Morris, M.A., Vangala, P., Jurczyk, A., Bortell, R., Harlan, D.M., Wang, J.P., and Nadler, J.L. (2017). Coxsackievirus-Induced Proteomic Alterations in Primary Human Islets Provide Insights for the Etiology of Diabetes. *J. Endocr. Soc.* *1*, 1272–1286.
- Djouder, N., Metzler, S.C., Schmidt, A., Wirbelauer, C., Gstaiger, M., Aebbersold, R., Hess, D., and Krek, W. (2007). S6K1-mediated disassembly of mitochondrial URI/PP1gamma complexes activates a negative feedback program that counters S6K1 survival signaling. *Mol. Cell* *28*, 28–40.
- Chaves-Pérez, A., Yilmaz, M., Perna, C., de la Rosa, S., and Djouder, N. (2019). URI is required to maintain intestinal architecture during ionizing radiation. *Science* *364*, eaaq1165.
- Gstaiger, M., Luke, B., Hess, D., Oakeley, E.J., Wirbelauer, C., Blondel, M., Vigneron, M., Peter, M., and Krek, W. (2003). Control of nutrient-sensitive transcription programs by the unconventional prefoldin URI. *Science* *302*, 1208–1212.
- Burén, S., Gomes, A.L., Teijeiro, A., Fawal, M.A., Yilmaz, M., Tummala, K.S., Perez, M., Rodríguez-Justo, M., Campos-Olivas, R., Megías, D., and Djouder, N. (2016). Regulation of OGT by URI in Response to Glucose Confers c-MYC-Dependent Survival Mechanisms. *Cancer Cell* *30*, 290–307.
- Ma, J., and Hart, G.W. (2013). Protein O-GlcNAcylation in diabetes and diabetic complications. *Expert Rev. Proteomics* *10*, 365–380.

28. Gomes, A.L., Teijeiro, A., Burén, S., Tummala, K.S., Yilmaz, M., Waisman, A., Theurillat, J.P., Perna, C., and Djouder, N. (2016). Metabolic Inflammation-Associated IL-17A Causes Non-alcoholic Steatohepatitis and Hepatocellular Carcinoma. *Cancer Cell* 30, 161–175.
29. Tummala, K.S., Gomes, A.L., Yilmaz, M., Graña, O., Bakiri, L., Ruppen, I., Ximénez-Embún, P., Sheshappanavar, V., Rodríguez-Justo, M., Pisano, D.G., et al. (2014). Inhibition of de novo NAD(+) synthesis by oncogenic URI causes liver tumorigenesis through DNA damage. *Cancer Cell* 26, 826–839.
30. Liu, S., Le May, C., Wong, W.P., Ward, R.D., Clegg, D.J., Marcelli, M., Korach, K.S., and Mauvais-Jarvis, F. (2009). Importance of extranuclear estrogen receptor-alpha and membrane G protein-coupled estrogen receptor in pancreatic islet survival. *Diabetes* 58, 2292–2302.
31. Mauvais-Jarvis, F. (2018). Gender differences in glucose homeostasis and diabetes. *Physiol. Behav.* 187, 20–23.
32. Toaima, D.N., El-Samahy, M.H., Zaki, O.K., Elshami, Y.M., and Toaima, N.N. (2020). Effect of estrogen receptor- alpha gene polymorphism (IVS1-397 T>C) on microvascular complications of type 1 diabetes mellitus. *Curr. Diabetes Rev.* 16, 770–778.
33. Roivainen, M., Rasilainen, S., Ylipaasto, P., Nissinen, R., Ustinov, J., Bouwens, L., Eizirik, D.L., Hovi, T., and Otonkoski, T. (2000). Mechanisms of coxsackievirus-induced damage to human pancreatic beta-cells. *J. Clin. Endocrinol. Metab.* 85, 432–440.
34. Drescher, K.M., Kono, K., Bopegamage, S., Carson, S.D., and Tracy, S. (2004). Coxsackievirus B3 infection and type 1 diabetes development in NOD mice: insulinitis determines susceptibility of pancreatic islets to virus infection. *Virology* 329, 381–394.
35. Spijker, H.S., Ravelli, R.B.G., Mommaas-Kienhuis, A.M., van Apeldoorn, A.A., Engelse, M.A., Zaldumbide, A., Bonner-Weir, S., Rabelink, T.J., Hoeben, R.C., Clevers, H., et al. (2013). Conversion of mature human β -cells into glucagon-producing α -cells. *Diabetes* 62, 2471–2480.
36. Merglen, A., Theander, S., Rubi, B., Chaffard, G., Wollheim, C.B., and Maechler, P. (2004). Glucose sensitivity and metabolism-secretion coupling studied during two-year continuous culture in INS-1E insulinoma cells. *Endocrinology* 145, 667–678.
37. Busse, N., Paroni, F., Richardson, S.J., Laiho, J.E., Oikarinen, M., Frisk, G., Hyöty, H., de Koning, E., Morgan, N.G., and Maedler, K. (2017). Detection and localization of viral infection in the pancreas of patients with type 1 diabetes using short fluorescently-labelled oligonucleotide probes. *Oncotarget* 8, 12620–12636.
38. Richardson, S.J., Leete, P., Dhayal, S., Russell, M.A., Oikarinen, M., Laiho, J.E., Svedin, E., Lind, K., Rosenling, T., Chapman, N., et al.; nPOD-V Consortium (2014). Evaluation of the fidelity of immunolabelling obtained with clone 5DB/1, a monoclonal antibody directed against the enteroviral capsid protein, VP1, in human pancreas. *Diabetologia* 57, 392–401.
39. Hingorani, A., and Ascher, E. (2003). Dyeless vascular surgery. *Cardiovasc. Surg.* 11, 12–18.
40. Tummala, K.S., Brandt, M., Teijeiro, A., Graña, O., Schwabe, R.F., Perna, C., and Djouder, N. (2017). Hepatocellular Carcinomas Originate Predominantly from Hepatocytes and Benign Lesions from Hepatic Progenitor Cells. *Cell Rep.* 19, 584–600.
41. Yang, Y.P., Thorel, F., Boyer, D.F., Herrera, P.L., and Wright, C.V.E. (2011). Context-specific α -to- β -cell reprogramming by forced Pdx1 expression. *Genes Dev.* 25, 1680–1685.
42. Xiao, X., Guo, P., Shiota, C., Zhang, T., Coudriet, G.M., Fischbach, S., Prasad, K., Fusco, J., Ramachandran, S., Witkowski, P., et al. (2018). Endogenous Reprogramming of Alpha Cells into Beta Cells, Induced by Viral Gene Therapy, Reverses Autoimmune Diabetes. *Cell Stem Cell* 22, 78–90.e4.
43. Chakravarthy, H., Gu, X., Enge, M., Dai, X., Wang, Y., Diamond, N., Downie, C., Liu, K., Wang, J., Xing, Y., et al. (2017). Converting Adult Pancreatic Islet α Cells into β Cells by Targeting Both Dnmt1 and Arx. *Cell Metab.* 25, 622–634.
44. Chera, S., Baronnier, D., Ghila, L., Cigliola, V., Jensen, J.N., Gu, G., Furuyama, K., Thorel, F., Gribble, F.M., Reimann, F., and Herrera, P.L. (2014). Diabetes recovery by age-dependent conversion of pancreatic δ -cells into insulin producers. *Nature* 514, 503–507.
45. Thorel, F., Népote, V., Avril, I., Kohno, K., Desgraz, R., Chera, S., and Herrera, P.L. (2010). Conversion of adult pancreatic alpha-cells to beta-cells after extreme beta-cell loss. *Nature* 464, 1149–1154.
46. Bramswig, N.C., Everett, L.J., Schug, J., Dorrell, C., Liu, C., Luo, Y., Stree-ter, P.R., Naji, A., Grompe, M., and Kaestner, K.H. (2013). Epigenomic plasticity enables human pancreatic α to β cell reprogramming. *J. Clin. Invest.* 123, 1275–1284.
47. Bertin, A., Sane, F., Gmyr, V., Lobert, D., Dechaumes, A., Kerr-Conte, J., Pattou, F., and Hober, D. (2019). Coxsackievirus-B4 Infection of Human Primary Pancreatic Ductal Cell Cultures Results in Impairment of Differentiation into Insulin-Producing Cells. *Viruses* 11, 597.
48. Oshima, M., Knoch, K.P., Diedisheim, M., Petzold, A., Cattani, P., Bugliani, M., Marchetti, P., Choudhary, P., Huang, G.C., Bornstein, S.R., et al. (2018). Virus-like infection induces human β cell dedifferentiation. *JCI Insight* 3, e97732.
49. Holland, A.M., Hale, M.A., Kagami, H., Hammer, R.E., and MacDonald, R.J. (2002). Experimental control of pancreatic development and maintenance. *Proc. Natl. Acad. Sci. USA* 99, 12236–12241.
50. Wu, K.L., Gannon, M., Peshavaria, M., Offield, M.F., Henderson, E., Ray, M., Marks, A., Gamer, L.W., Wright, C.V., and Stein, R. (1997). Hepatocyte nuclear factor 3beta is involved in pancreatic beta-cell-specific transcription of the pdx-1 gene. *Mol. Cell. Biol.* 17, 6002–6013.
51. Melloul, D., Marshak, S., and Cerasi, E. (2002). Regulation of insulin gene transcription. *Diabetologia* 45, 309–326.
52. Yang, B.T., Dayeh, T.A., Volkov, P.A., Kirkpatrick, C.L., Malmgren, S., Jing, X., Renström, E., Wollheim, C.B., Nitert, M.D., and Ling, C. (2012). Increased DNA methylation and decreased expression of PDX-1 in pancreatic islets from patients with type 2 diabetes. *Mol. Endocrinol.* 26, 1203–1212.
53. Park, J.H., Stoffers, D.A., Nicholls, R.D., and Simmons, R.A. (2008). Development of type 2 diabetes following intrauterine growth retardation in rats is associated with progressive epigenetic silencing of Pdx1. *J. Clin. Invest.* 118, 2316–2324.
54. Oghamian, S., Sodir, N.M., Bashir, M.U., Shen, H., Cullins, A.E., Carroll, C.A., Kundu, P., Shibata, D., and Laird, P.W. (2011). Reduction of pancreatic acinar cell tumor multiplicity in Dnmt1 hypomorphic mice. *Carcinogenesis* 32, 829–835.
55. Shi, J.F., Li, X.J., Si, X.X., Li, A.D., Ding, H.J., Han, X., and Sun, Y.J. (2012). ER α positively regulated DNMT1 expression by binding to the gene promoter region in human breast cancer MCF-7 cells. *Biochem. Biophys. Res. Commun.* 427, 47–53.
56. Ku, J.L., Park, S.C., Kim, K.H., Jeon, Y.K., Kim, S.H., Shin, Y.K., Noh, D.Y., Im, S.A., Bang, Y.J., Han, W., et al. (2013). Establishment and characterization of seven human breast cancer cell lines including two triple-negative cell lines. *Int. J. Oncol.* 43, 2073–2081.
57. Zhang, Y., and Wang, L. (2011). Nuclear receptor SHP inhibition of Dnmt1 expression via ERR γ . *FEBS Lett.* 585, 1269–1275.
58. Lee, B.H., Yegnasubramanian, S., Lin, X., and Nelson, W.G. (2005). Pro-cainamide is a specific inhibitor of DNA methyltransferase 1. *J. Biol. Chem.* 280, 40749–40756.
59. Reimer, M.K., and Ahrén, B. (2002). Altered beta-cell distribution of pdx-1 and GLUT-2 after a short-term challenge with a high-fat diet in C57BL/6J mice. *Diabetes* 51 (Suppl 1), S138–S143.
60. Fujimoto, K., Ford, E.L., Tran, H., Wice, B.M., Crosby, S.D., Dorn, G.W., 2nd, and Polonsky, K.S. (2010). Loss of Nix in Pdx1-deficient mice prevents apoptotic and necrotic β cell death and diabetes. *J. Clin. Invest.* 120, 4031–4039.

61. Lin, Y., and Sun, Z. (2015). In vivo pancreatic β -cell-specific expression of antiangiogenic gene Klotho: a novel approach for preserving β -cells in type 2 diabetes. *Diabetes* 64, 1444–1458.
62. Hober, D., and Sauter, P. (2010). Pathogenesis of type 1 diabetes mellitus: interplay between enterovirus and host. *Nat. Rev. Endocrinol.* 6, 279–289.
63. Richardson, S.J., Willcox, A., Bone, A.J., Foulis, A.K., and Morgan, N.G. (2009). The prevalence of enteroviral capsid protein vp1 immunostaining in pancreatic islets in human type 1 diabetes. *Diabetologia* 52, 1143–1151.
64. Masini, M., Martino, L., Marselli, L., Bugliani, M., Boggi, U., Filippini, F., Marchetti, P., and De Tata, V. (2017). Ultrastructural alterations of pancreatic beta cells in human diabetes mellitus. *Diabetes Metab. Res. Rev.* 33. <https://doi.org/10.1002/dmrr.2894>.
65. Piran, R., Lee, S.H., Kuss, P., Hao, E., Newlin, R., Millán, J.L., and Levine, F. (2016). PAR2 regulates regeneration, transdifferentiation, and death. *Cell Death Dis.* 7, e2452.
66. Yeung, W.C., Rawlinson, W.D., and Craig, M.E. (2011). Enterovirus infection and type 1 diabetes mellitus: systematic review and meta-analysis of observational molecular studies. *BMJ* 342, d35.
67. Diamond, N., Engler, S., Zanotelli, V.R.T., Schapiro, D., Wasserfall, C.H., Kusmartseva, I., et al. (2019). A Map of Human Type 1 Diabetes Progression by Imaging Mass Cytometry. *Cell Metab.* 29, 755–768.e5.
68. Wang, Y.J., Traum, D., Schug, J., Gao, L., Liu, C., HPAP Consortium; Atkinson, M.A., Powers, A.C., Feldman, M.D., Naji, A., et al. (2019). Multiplexed In Situ Imaging Mass Cytometry Analysis of the Human Endocrine Pancreas and Immune System in Type 1 Diabetes. *Cell Metab.* 29, 769–783.e4.
69. Liang, T., Dolai, S., Xie, L., Winter, E., Orabi, A.I., Karimian, N., Cosen-Binker, L.I., Huang, Y.C., Thorn, P., Cattral, M.S., and Gaisano, H.Y. (2017). *Ex vivo* human pancreatic slice preparations offer a valuable model for studying pancreatic exocrine biology. *J. Biol. Chem.* 292, 5957–5969.
70. Sickles, G.M., Feorino, P., and Plager, H. (1955). Isolation and type determination of Coxsackie virus, group B, in tissue culture. *Proc. Soc. Exp. Biol. Med.* 88, 22–24.
71. Chapman, N.M., Kim, K.S., Drescher, K.M., Oka, K., and Tracy, S. (2008). 5' terminal deletions in the genome of a coxsackievirus B2 strain occurred naturally in human heart. *Virology* 375, 480–491.
72. Neiman, D., Moss, J., Hecht, M., Magenheimer, J., Piyanzin, S., Shapiro, A.M.J., de Koning, E.J.P., Razin, A., Cedar, H., Shemer, R., and Dor, Y. (2017). Islet cells share promoter hypomethylation independently of expression, but exhibit cell-type-specific methylation in enhancers. *Proc. Natl. Acad. Sci. USA* 114, 13525–13530.
73. Thaiss, C.A., Levy, M., Grosheva, I., Zheng, D., Soffer, E., Blacher, E., Braverman, S., Tengeler, A.C., Barak, O., Elazar, M., et al. (2018). Hyperglycemia drives intestinal barrier dysfunction and risk for enteric infection. *Science* 359, 1376–1383.
74. Chen, C., Fang, R., Davis, C., Maravelias, C., and Sibley, E. (2009). Pdx1 inactivation restricted to the intestinal epithelium in mice alters duodenal gene expression in enterocytes and enteroendocrine cells. *Am. J. Physiol. Gastrointest. Liver Physiol.* 297, G1126–G1137.
75. Cinti, F., Bouchi, R., Kim-Muller, J.Y., Ohmura, Y., Sandoval, P.R., Masini, M., Marselli, L., Suleiman, M., Ratner, L.E., Marchetti, P., and Accili, D. (2016). Evidence of β -cell dedifferentiation in human type 2 diabetes. *J. Clin. Endocrinol. Metab.* 101, 1044–1054.
76. Ziv, O., Glaser, B., and Dor, Y. (2013). The plastic pancreas. *Dev. Cell* 26, 3–7.
77. Wang, Z., York, N.W., Nichols, C.G., and Remedi, M.S. (2014). Pancreatic β cell dedifferentiation in diabetes and redifferentiation following insulin therapy. *Cell Metab.* 19, 872–882.
78. Chee, Y.J., Ng, S.J.H., and Yeoh, E. (2020). Diabetic ketoacidosis precipitated by Covid-19 in a patient with newly diagnosed diabetes mellitus. *Diabetes Res. Clin. Pract.* 164, 108166.
79. Rubino, F., Amiel, S.A., Zimmet, P., Alberti, G., Bornstein, S., Eckel, R.H., Mingrone, G., Boehm, B., Cooper, M.E., Chai, Z., et al. (2020). New-Onset Diabetes in Covid-19. *N. Engl. J. Med.* 383, 789–790.
80. Yang, J.K., Lin, S.S., Ji, X.J., and Guo, L.M. (2010). Binding of SARS coronavirus to its receptor damages islets and causes acute diabetes. *Acta Diabetol.* 47, 193–199.
81. Lee, J.Y., Ristow, M., Lin, X., White, M.F., Magnuson, M.A., and Hennighausen, L. (2006). RIP-Cre revisited, evidence for impairments of pancreatic β -cell function. *J. Biol. Chem.* 281, 2649–2653.
82. Srinivas, S., Watanabe, T., Lin, C.S., William, C.M., Tanabe, Y., Jessell, T.M., and Costantini, F. (2001). Cre reporter strains produced by targeted insertion of EYFP and ECFP into the ROSA26 locus. *BMC Dev. Biol.* 1, 4.
83. Zhang, Y., Proenca, R., Maffei, M., Barone, M., Leopold, L., and Friedman, J.M. (1994). Positional cloning of the mouse obese gene and its human homologue. *Nature* 372, 425–432.
84. Flatt, P.R., and Bailey, C.J. (1981). Abnormal plasma glucose and insulin responses in heterozygous lean (ob/+) mice. *Diabetologia* 20, 573–577.
85. Carter, J.D., Dula, S.B., Corbin, K.L., Wu, R., and Nunemaker, C.S. (2009). A practical guide to rodent islet isolation and assessment. *Biol. Proced. Online* 11, 3–31.
86. Fawal, M.A., Brandt, M., and Djouder, N. (2015). MCRS1 binds and couples Rheb to amino acid-dependent mTORC1 activation. *Dev. Cell* 33, 67–81.
87. Bock, C., Reither, S., Mikeska, T., Paulsen, M., Walter, J., and Lengauer, T. (2005). BiQ Analyzer: visualization and quality control for DNA methylation data from bisulfite sequencing. *Bioinformatics* 21, 4067–4068.

STAR★METHODS

KEY RESOURCES TABLE

REAGENT or RESOURCE	SOURCE	IDENTIFIER
Antibodies		
Alexa Fluor 488 Goat anti-Chicken IgY (H+L)	Life Technologies	A-11039; RRID:AB_2534096
Alexa Fluor 488 Goat anti-Mouse IgG	Life Technologies	A-11001; RRID:AB_2534069
Alexa Fluor 488 Donkey anti-Mouse IgG	Life Technologies	A-21202; RRID:AB_141607
Alexa Fluor 555 Goat anti-Mouse IgG	Life Technologies	A-21422; RRID:AB_2535844
Alexa Fluor 555 Goat anti-Rabbit IgG	Life Technologies	A-21429; RRID:AB_2535850
Alexa Fluor 555 Donkey anti-Goat IgG	Life Technologies	A-21432; RRID:AB_2535853
Alexa Fluor 647 Goat anti-Rabbit IgG (H+L)	Life Technologies	A-21245; RRID:AB_2535813
Alexa Fluor 647 Donkey anti-Rabbit IgG	Life Technologies	A-31573; RRID:AB_2536183
Goat Polyclonal anti-Mouse HRP conjugated	Dako	P0447; RRID:AB_2617137
Goat Polyclonal anti-Mouse AP conjugated	Sigma-Aldrich	A0168; RRID:AB_257867
Goat Polyclonal anti-Rabbit HRP conjugated	Dako	P0448; RRID:AB_2617138
Goat polyclonal anti-PDX1	R&D Systems	AF2419; RRID:AB_355257
Mouse BD Fc block	BD BioSciences	553141; RRID:AB_394656
Mouse monoclonal anti-ER α	Santa Cruz Biotechnology	Sc-8002; RRID:AB_627558
Mouse monoclonal anti-Glucagon	Sigma-Aldrich	G2654; RRID:AB_259852
Mouse monoclonal anti-HA Tag (16B12)	BioLegend	MMS-101R; RRID:AB_291262
Mouse monoclonal anti-PDX1	R&D Systems	MAB2419; RRID:AB_2268098
Mouse monoclonal anti-URI	This paper	N/A
Mouse monoclonal anti-Vinculin	Sigma	V9131; RRID:AB_477629
Mouse monoclonal anti-VP1	Dako	M7064; RRID:AB_2118128
Rabbit polyclonal anti-Caspase 3	Cell Signaling Technology	9662; RRID:AB_331439
Rabbit monoclonal anti-GST	Sigma	G7781; RRID:AB_259965
Rabbit monoclonal anti-HSP90	Cell Signaling Technology	4877; RRID:AB_2233307
Rabbit monoclonal anti-Ki67 (SP6)	Master Diagnostica	MAD-000310QD
Rabbit polyclonal anti-URI	This paper	N/A
Rabbit polyclonal anti-Chromogranin A	Abcam	ab15160; RRID:AB_301704
Rabbit polyclonal anti-DNMT1	Santa Cruz Biotechnology	sc-20701; RRID:AB_2293064
Rabbit polyclonal anti-Glut2	Novus Biologicals	NBP2-22218; RRID:AB_2335858
Rabbit polyclonal anti-Insulin	Cell Signaling Technology	4590; RRID:AB_659820
Bacterial and Virus Strains		
CVB4 JVB	ATCC	VR-184#
Biological Samples		
Human diabetic pancreatic samples	CNIO Biobank, Biobanc-Mur, MarBiobank, Vasque Biobank, Andalusian Public Health System Biobank, and Biobank of IDIBAPS.	N/A
Human primary islets	Prodo Laboratories, Inc	¹¹
Chemicals, Peptides, and Recombinant Proteins		
2-mercaptoethanol	Sigma Aldrich	M3148
2-Propanol 99,7%	Panreac Quimica	11610901214
30%(w/v) Acrylamide: 0.8% /9w/v) Bis-Acrylamide Stock Solution (37.5:1)	ProtoGel	EC-890
Acetic Acid	Fisher Scientific	100063.1000
Agarose Electrophoresis Grade	Apollo Scientific	BIA1176
Aprotinin	Sigma Aldrich	A1153

(Continued on next page)

Continued

REAGENT or RESOURCE	SOURCE	IDENTIFIER
Aqua Live Dead	Life Technologies	L34957
Blotting-Grade Blocker	BioRad	170-6404
BD Cytotfix	BD BioSciences	51-2090KZ
BD Perm/Wash	BD BioSciences	51-2091KZ
Bovine Serum Albumin	Sigma Aldrich	A7906
Bradford Protein Assay	BioRad	5000001
Bromophenol Blue	Sigma Aldrich	B0126
Citric Acid 500 g	Sigma Aldrich	C0759
Chloroform	Sigma Aldrich	C2432
Collagenase P	Roche	11213857001
Coomassie Brilliant Blue	BioRad	161-0436
Complete TM , EDTA-free Protease Inhibitor Cocktail	Roche	COEDTAF-RO
D-Glucose 250 g	Sigma Aldrich	G7528
DAPI 4.6-diamidino-2-phenylindole 5 mg	Sigma Aldrich	D9542
DMEM	Life Technologies, S.A.	31885-049
DMSO	Sigma Aldrich	D8418
DNase I recombinant, RNase-free	Roche	04716728001
Doxycycline 1g	Sigma Aldrich	D9891
DTT (Dithiothreitol)	Sigma Aldrich	D9779
EcoRI Digestion Enzyme	New England Biolabs	R0101S
EcoRV Digestion Enzyme	New England Biolabs	R3195M
EDTA (Ethylenediaminetetraacetic acid)	Sigma Aldrich	ED
EGTA (Ethylene glycol-bis(2-aminoethylether)-N, N, N, N-tetraacetic acid)	Sigma Aldrich	E3889
Ethanol 96%	Panreac Quimica	141085.1214
Fetal Bovine Serum	Sigma Aldrich	F7524-500ML
FITC/Dextran	Sigma Aldrich	46945
Formalin solution 10%	Panreac Quimica S.L.U.	HT501128
Forskolin	Sigma Aldrich	F6886
Glutamax Supplement 200mM GIBCO	Life Technologies, S.A.	35050-038
Gluthathione Sepharose 4 Fast Flow	GE Healthcare	17-5132-01
Glycerol	Sigma Aldrich	G5516
Hematoxylin	Panreac Quimica, S.L.U.	2552981610
HEPES	Life Technologies, S.A.	15630-049
Hydrogen Peroxide Solution 500 ml	Sigma Aldrich	H1009
LB Agar /20 Plates (Free antibiotics)	Laboratorios Conda, S.A.	10354
Liquid DAB + Substrate Chromogen System	Dako	K3468
Luminol (97%)	Sigma Aldrich	123072
Magnesium Chloride (MgCl ₂)	Sigma Aldrich	208337
NaCl (Sodium Chloride)	Sigma Aldrich	S9625
NP-40 Alternative	Calbiochem	D00120899
p-Coumaric Acid	Sigma Aldrich	C9008
Paraformaldehyde	Electron Microscopy Sciences	19202
PBS 10X (For IHC/IF)	ALAOS	PB515M-10
PBS w/o Ca ²⁺ / Mg ²⁺ (For tissue culture)	Cultek S.L.U.	BE-17516F
Penicillin-Streptomycin 100ML GIBCO	Life Technologies, S.A.	15070-063
PMSF (Phenylmethylsulfonyl Fluoride)	Sigma Aldrich	P7626
Propidium iodide	Sigma Aldrich	P4170
Potassium Chloride	Sigma Aldrich	P9541

(Continued on next page)

Continued

REAGENT or RESOURCE	SOURCE	IDENTIFIER
Procinamide hydrochloride, 99%	Fischer Scientific	10167743
Protein A Sepharose 4 Fast Flow	GE Healthcare	17-1279-01
Protein G Sepharose 4 Fast Flow	GE Healthcare	17-0618-01
Proteinase K	VWR Internacional Eurolab, S.L.	0706-100 mg
Prolong Gold Antifade Reagent 10 ml	Life Technologies	P36930
Resazurin Sodium Salt	Sigma Aldrich	R7017
Rnase A solution	Sigma Aldrich	R6148
SDS (Sodium dodecyl sulfate)	BioRad	1610302
Sodium Citrate Tribasic Dihydrate	Sigma Aldrich	S4641
Sodium Deoxycholate	Sigma Aldrich	D6750
Sodium Fluoride	Sigma Aldrich	S7920
Sodium Orthovanadate	Sigma Aldrich	S6508
Sodium Phosphate Dibasic	Sigma Aldrich	S3264
Sodium Pyrophosphate Tetrabasic	Sigma Aldrich	S6422
Sunflower seed oil from Helianthus annuus	Sigma Aldrich	88921-1L-F
TAE 50X (Tris-Acetic Acid-EDTA)	ALAOs	TA475M
Tolbutamide	Sigma Aldrich	T0891
Triton X-100	Sigma Aldrich	T8787
Trizma Base	Sigma Aldrich	T1503
Tween 20	Sigma Aldrich	P7949
Critical Commercial Assays		
AmpONE™ Taq DNA polymerase	GeneAll	501-050
Avidin/ Biotin Blocking Kit	Vector Laboratories	SP-2001
Bradford Protein Assay Kit	Bio-Rad	5000006
Catalase Activity Assay Kit	Abcam	ab83464
Dako Fluorescence Mounting Medium	DAKO	S3023
FuGENE HD Transfection Reagent	Promega	E2311
GenElute™ HP Plasmid Midiprep	Sigma Aldrich	NA0200S
GoTaq qPCR Master Mix	Promega	A6002
<i>In Situ</i> Cell Death Detection Kit, Fluorescein	Roche	11684795910
Lipofectamine 2000 Transfection Reagent	Thermo Fisher	11668019
Lipofectamine RNAiMAX Transfection Reagent	Thermo Fisher	13778100
M-MLV Reverse Transcriptase	Life Technologies	28025013
Mouse on Mouse (M.O.M.) Basic Kit	Vector Laboratories	BMK-2202
Prime-It II Random Primer Labeling Kit	Agilent Technologies	300385
QIAquick Gel Extraction Kit	QIAGEN	28704
QIAquick PCR Purification Kit	QIAGEN	28104
SIGMAFAST Fast Red TR/Naphthol AS-MX	Sigma Aldrich	F4648
SuperScript VIL0 cDNA Synthesis Kit and Master Mix	Life Technologies	11754050
TNT T7 Coupled Reticulocyte Lysate System	Promega	L1170
TSA™ Plus Biotin Kit	PerkinElmer	NEL749A001KT
Ultrasensitive Mouse Insulin ELISA	Mercodia	10-1249-01
Glucagon EIA kit	Sigma Aldrich	RAB0202-1KT
Vectastain ABC HRP Kit (Peroxidase, Goat IgG)	Vector Laboratories	PK-4005
Vectastain ABC HRP Kit (Peroxidase, Mouse IgG)	Vector Laboratories	PK-4002
Vectastain ABC HRP Kit (Peroxidase, Rabbit IgG)	Vector Laboratories	PK-4001
Vectastain ABC HRP Kit (Peroxidase, Rat IgG)	Vector Laboratories	PK-4004

(Continued on next page)

Continued

REAGENT or RESOURCE	SOURCE	IDENTIFIER
Experimental Models: Cell Lines		
293T cells (HEK)	ATCC	CRL-3216
MCF7 cells	ATCC	HTB-22TM
INS-1E cells	36	N/A
INS-1 cells	36	N/A
Experimental Models: Organisms/Strains		
NOD/Cg-Prkdc ^{scid} IL2rg ^{tm1WJL} Tg(<i>Ins2</i> -HBEGF) 6832Ugfm/Sz	University of Massachusetts Medical School (UMMS)	J:225120
<i>Pdx1</i> ^{flTA} mouse: 129X1/SvJ- <i>Pdx1</i> ^{tm1Macd}	Spanish National Cancer Research Centre (CNIO)	J:79206
<i>Pdx1-cre</i> mouse: FVB/N- Tg(<i>Pdx1-cre</i>)6Tuv	Spanish National Cancer Research Centre (CNIO)	J:87973
Rosa26LSLYFP: 129X1/SvJ- Gt(<i>Rosa</i>)26Sor ^{tm1(EYFP)} Cos	Spanish National Cancer Research Centre (CNIO)	J:80963
<i>Col1a1</i> ^{tm1(tetO-URI1)Ndj}	Spanish National Cancer Research Centre (CNIO)	J:217463
<i>Uri1</i> ^{tm1.1Ndj}	Spanish National Cancer Research Centre (CNIO)	J:217463
Oligonucleotides		
Primers For ChIP, see Table S3	This Paper	N/A
Primers For Bisulfite Sequencing, see Table S4	This Paper	N/A
Primers For Genotyping, see Table S5	This Paper	N/A
Primers For qRT-PCR, see Table S5	This Paper	N/A
ON-TARGETplus Non-Targeting Pool	Dharmacon	D-001810-10
ON-TARGETplus Human URI1 siRNA	Dharmacon	L-017399-00
siGLO green transfection indicator	Dharmacon	D-001630-01
<i>Uri1</i> -siRNA1: CUGAGGCAAAGUAGCUUUAUAdAdA,	Origene	SR502040
<i>Uri1</i> -siRNA2: CUAAGUGGCAAAGCAUGAAGUGUdCdT	Origene	SR502040
<i>Uri1</i> -siRNA3: UGGUUCUUAUAAAGCUUACGCUgTdA	Origene	SR502040
Recombinant DNA		
pGEX-4T-1-URI (1-267)	This Paper	N/A
pGEX-4T-1-URI (1-534)	This Paper	N/A
pGEX-4T-1-URI (156-534)	This Paper	N/A
pGEX-4T-1-URI (1-517)	This Paper	N/A
pGEX-4T-1-URI (282-534)	This Paper	N/A
pGEX-4T-1-URI (390-534)	This Paper	N/A
pGEX-4T-1-URI (466-534)	This Paper	N/A
pGEX-4T-1-URI (156-283)	This Paper	N/A
pGEX-4T-1-URI (1-158)	This Paper	N/A
pcDNA3.1-hURI (1-534)	This Paper	N/A
pcDNA3.1-hURI (1-193)	This Paper	N/A
pcDNA3.1-hURI (194-389)	This Paper	N/A
pcDNA3.1-hURI (390-534)	This Paper	N/A
<u>pTK-CAT</u>	50	N/A
<u>pTK-pdx1.1-CAT</u>	50	N/A
<u>pTK-pdx1.2-CAT</u>	50	N/A
<u>pTK-pdx1.3-CAT</u>	50	N/A
<u>pTK-pdx1.4-CAT</u>	50	N/A

(Continued on next page)

Continued

REAGENT or RESOURCE	SOURCE	IDENTIFIER
pTK-pdx1.5-CAT	50	N/A
pTK-pdx1.6-CAT	50	N/A
Software and Algorithms		
ImageJ 1.7v	NIH	https://imagej.nih.gov/ij/
Prism 5	GraphPad Software	https://www.graphpad.com
Gen5 software	BioTek	https://www.biotek.com/products/software-robotics-software/gen5-microplate-reader-and-imager-software/
Other		
Precellys 24 Bead Mill homogenizer	Bertin Technologies	Equation 03119-200-RD000.0
Accu-Chek Aviva Glucometer	Roche Diagnostics	200602
Accu-Chek Aviva Glucose strips	Roche Diagnostics	6916678001
Amersham Protran 0.2 μm NC	GE Healthcare	10600001
Chow diet - 18% fat, 58% carbohydrates, and 24% proteins	Harlan Laboratories	2018S
Doxycycline Hyclate diet (200 mg/ Kg)	Envigo	TD.04104
High fat diet - 45% fat, 35% carbohydrates, and 20% proteins	Research Diets	D12451

RESOURCE AVAILABILITY

Lead Contact

Further information and requests for resources and reagents should be directed to and will be fulfilled by the Lead Contact, Nabil Djouder (ndjouder@cniio.es).

Materials Availability

Materials are available upon request to N.D. Mouse lines generated in the lab will be subjected to standard material transfer agreements.

Data and Code Availability

This study did not generate any unique datasets or code.

EXPERIMENTAL MODEL AND SUBJECT DETAILS

Mouse Models

To engraft the islets NSG (NOD/Cg-Prkdc^{scid} IL2rg^{tm1WJL} Tg(*Ins2*-HBEGF)6832Ugfm/Sz) were used as previously described.¹¹

To specifically express human URI (*hURI1*^(+/KI)) in the pancreas, ColhURI (WT) mouse previously described²⁹ was crossed with a line containing the tetracycline-dependent transactivator (tTA) under the control of the *Pdx1* promoter - i.e., *Pdx1*^(tTA/+) mouse⁴⁹ - to generate *hURI1*^(+/KI); *Pdx1*^(tTA/+) mouse. Pancreatic-specific ectopic *hURI1* expression was allowed since embryonic stage E8.5 when *Pdx1* gene expression starts.

To induce URI deletion specifically in β cells, URI lox mouse previously described²⁴ was crossed with a line containing the Cre recombinase under the control of *Pdx1* promoter - i.e, Tg(*Pdx1*-cre)6Tuv mouse³⁹ - generating the *Uri1*^{lox/lox} (also named as *Uri1*^{+/+}, as no phenotype was observed in this mice), *Uri1*^{lox/+}; *Pdx1*-cre and *Uri1*^{lox/lox}; *Pdx1*-cre mice, respectively

To re-induce URI expression in URI-deleted pancreas, *Uri1*^{lox/lox}; *Pdx1*-cre mouse was crossed with the *hURI1*^(+/KI); *Pdx1*^(tTA/+) mouse in order to generate the *hURI1*^(+/KI); *Pdx1*^(tTA/+); *Uri1*^{lox/lox}; *Pdx1*-cre mouse.

To express EYFP in URI-deleted pancreas, *Uri1*^{lox/lox}; *Pdx1*-cre mouse was crossed with the R26R-EYFP mouse,⁸² previously reported and present in house in order to generate the *Uri1*^{lox/lox}; *Pdx1*-cre; R26R-EYFP mouse.

To induce URI deletion specifically in β cells in adult mice, 8 to 10 weeks old *hURI1*^(+/KI); *Pdx1*^(tTA/+); *Uri1*^{lox/lox}; *Pdx1*-cre mice were treated continuously with doxycycline diet.

hURI1^(+/KI); *Pdx1*^(tTA/+) mouse was crossed with *ob/+* (B6.V-Lepob/J) mouse (Jackson lab)⁸³ to generate the *ob/+*; *hURI1*^(+/KI); *Pdx1*^(tTA/+) mouse. *ob/+* mouse has been described to have glucose impaired response and hyperinsulinemia.⁸⁴

CVB4-Infected Mice Grafted with Human Islets

Coxsackievirus (CVB4)-infected and non-infected human islets engrafted in NOD/Cg-Prkdc^{scid} IL2rg^{tm1WJL} Tg(*Ins2*-HBEGF) 6832Ugfm/Sz (NSG-Tg(RIP-DTR)) mouse paraffin samples were kindly provided by Jennifer Wang, MD, University of Massachusetts Medical School (UMMS).¹¹ In short, immunodeficient and diabetes-prone NSG mice with transgenic expression of the diphtheria toxin receptor were treated with Diphtheria Toxin to induce hyperglycemia and loss of the murine β cell pool. Diabetic mice were then engrafted in two experiments with 3000 human islets in each mouse from one single, distinct human donor in each experiment. Human islet grafts are from two independent experiments (Exp 2 and Exp 3),¹¹ and were originally obtained from the Integrated Islet Distribution Program under protocols approved by the Institutional Review Board of the University of Massachusetts Medical School. These islets were transplanted in the mouse kidney in order to restore normoglycemia and were infected with CVB4. Briefly, mice were intraperitoneally injected with normal saline solution (Mock) or 1×10^4 plaque-forming units (pfu) of CVB4 strain JVB. Parameters on body weights and, blood glucose and insulin and C peptide levels are reported in Table S1. Paraffin-embedded samples from human islets were performed either at humane end point or end of the experiment (day 44 or day 49 for Exp 2 and Exp 3, respectively). Samples for experiments 2 and 3 were pooled in order to obtain statistical significance. No obvious changes in serum C-peptides, blood insulin levels, insulin mRNA expression or insulin/glucagon positive cell ratio in the mock samples were found between both experiments.¹¹

Human Islets for the Experiments *In Vitro*

Human primary islets were kindly provided by Jennifer Wang, MD, University of Massachusetts Medical School (UMMS) as described. In short, primary human islets from adult donors without diabetes were obtained from Prodo Laboratories, Inc. (Aliso Viejo, CA). Donor #17092 is a 44-year-old male African American with a BMI of 31 and a 4.7% glycated hemoglobin (HbA1c). Donor # 18200 is a 61-year-old female from a non-documented race with a BMI of 28.9 and a 5.6% glycated hemoglobin (HbA1c).

Human Pancreatic Samples

Human diabetic pancreatic samples and data were obtained from the CNIO Biobank thanks to the help of Maria-Jesus Artiga and from Biobanc-Mur, MarBiobank, Vasque Biobank and Andalusian Public Health System Biobank, integrated in the Spanish Biobank Network and funded by Instituto de Salud Carlos III. We are also thankful to the Biobank of IDIBAPS, Barcelona, to provide samples to Dr. Anna Novials. Samples were processed following standard operating procedures with the appropriate approval of the Ethics and Scientific Committees. Males and females were included in the study as indicated. Additional details on donors are provided in Table S2.

Cell Lines

INS-1, INS-1E, MCF-7 and HEK293T cells were maintained in high-glucose DMEM supplemented with glutamine, 10% (MCF-7 and HEK293T cells) or 15% (INS-1E cells) fetal bovine serum (FBS) and 100 units/ml penicillin and 0.1 mg/ml streptomycin. Cells were passed when 50% (INS-1E cells) or 80% (MCF-7 and HEK293T cells) of confluence was reached to maintain high proliferation potential.

METHOD DETAILS

Mouse Handling

All mice were housed in pathogen-free conditions. No inclusion criteria were used. The mice were housed with a 12-hour light/dark cycle between 8:00 and 20:00 in a temperature-controlled room ($22 \pm 1^\circ\text{C}$). All experiments were approved by the CNIO-ISCIII Ethics Committee and Community of Madrid (CAM) and performed in accordance with the guidelines for ethical conduct in the care and use of animals as stated in the international guiding principles for biomedical research involving animals, developed by the Council for International Organizations of Medical Sciences. Littermates were always used as controls. Males and females were respectively used for the study. Age/developmental stage of mice is included appropriately in the text and Figure Legends. Food (Harlan Laboratories and Research Diets Inc.) and water were provided *ad libitum*, unless described elsewhere.

Mouse Diets and Treatments

Mice were fed either with chow diet (18% fat, 58% carbohydrates, and 24% proteins) (Harlan Laboratories, 2018S), doxycycline hyclate diet (200 mg/ Kg) (TD.04104, ENVIGO) at concentration of 50 mg/kg or high-fat-diet (HFD) (45% fat, 35% carbohydrates, and 20% proteins) (Research Diets, D12451).

Procainamide (ARCOS, 10167743) was purchased from Fisher Scientific S.L. and stored under manufacturer's conditions. Procainamide was dissolved in water at the concentration of 0,32 g/kg and used as oral treatment to breeding pairs and weaned mice. The solution was changed every second day, freshly prepared and filtered.

Isolation of Mouse Pancreatic Islets

Mice pancreatic islets were obtained by Treatment by Collagenase P of Bile duct cannulated pancreases followed by density gradient with Histopaque 1100 as described previously.⁸⁵ In short, bile duct cannulated mice were injected with collagenase-P

(1,4mg/ml) in G solution (0.35 g NaHCO₃/L, 0.35 g NaHCO₃/L in HBSS) up to 5 mL to inflate all pancreatic lobes and placed into 15 mL centrifuge tube on ice. Pancreases were then incubated in a water bath at 37°C for 10 minutes and hand-shaken hard for 5 s and placed back on ice, filled up to 15 mL of G solution to slow digestive process. Digested pancreases were washed twice by centrifugation for 5 minutes at 300 g at room temperature, discarding supernatant and adding 10 mL of G solution. Pancreases were then passed through 100 μm strainers into 50 mL centrifuge tubes, and added additional 10 mL of G solution. Supernatant were discarded. Pellets were resuspended in 10 mL Histopaque 1100 solution and 10 mL of G solution was added with precaution so as to not disrupt Histopaque – G solution phases. Pancreas were the centrifuged at 900 g for 20 minutes at room temperature with no brake setting. After centrifugation islets at the interphase are collected and transferred to a new tube and 25 mL of G solution is added.

Tubes are washed by flushing with G solution and centrifuged at 450 g for 4 minutes at room temperature. Another round of washings is done by adding 10 mL of G solution and centrifugation at 450 g for 4 minutes at room temperature. Finally, pellets were resuspended with Culture solution (RPMI 1640, 10% fetal calf serum, penicillin (100 U/mL)/streptomycin (100 μg/mL).

Insulin Secretion Test (IST) in Isolated Islets

10 Pancreatic isolated islets per condition were hand-picked and pre-incubated in 1 mL Krebs–Ringer bicarbonate buffer supplemented with 2.8 mmol l⁻¹ glucose and 0.5% BSA at 37°C in an atmosphere of 5% CO₂–95% O₂ for 1 hour. Islets were then glucose stimulated by 16.7 mmol l⁻¹ glucose or not and in the presence or absence of different activators of insulin secretion for 30 minutes. Islets were then harvested and pelleted by centrifugation. Supernatants were taken for insulin release quantification.

Glucose Tolerance Test (GTT) in Mice

Mice were fasted for 6 hours and weighed. Blood glucose levels were determined doing a distal cut in the tail and placing a drop of blood in a test strip of a glucometer (ACCU-Check). A solution of 2 g of glucose/kg of body mass as administered by intraperitoneal (IP) injection. Blood glucose levels were measured at 0, 15, 30, 60 and 90 min in all cases and 120 min and 150 min in HFD-treated mice.

Insulin Tolerance Test (ITT) in Mice

Mice were fasted for 6 hours and weighed. Blood glucose levels were determined doing a distal cut in the tail and placing a drop of blood in a test strip of a glucometer (ACCU-Check). A solution of 0.75 U of IU/g of body mass as administered by intraperitoneal (IP) injection. Blood glucose levels were measured at 0, 15, 30, 60 and 90 min in all cases and 120 min in HFD-treated mice.

Insulin Secretion Test (IST) in Mice

Blood samples collected from the submandibular vein at 0 and 30 minutes respectively before and after intraperitoneal injection of 2 g of glucose/kg of body mass, placed in heparin tube and centrifuged 15 min at 3000 g. 25 μL of plasma were utilized to measure insulin levels using an enzyme-linked immunosorbent assay (ELISA) kit (Merckodia, 10-1249-01) for mouse insulin.

Plasmid Transfection and siRNA Experiments

URI overexpression experiments in INS-1, INS-1E and HEK293T cells were performed using pcDNA3-HA-URI and pcDNA3-HA as control.²⁶ Plasmids were transfected using FuGENE 6 in HEK293T cells and using Lipofectamine2000 in INS-1 and INS-1E cells, according to the manufacturer's instructions. Cells were analyzed 48-hour post-transfection.

Knockdown experiments in HEK293T cells were performed using ON-TARGET plus SMART pool siRNA targeting human URI (L-017399-00) as well as control siRNA (D-001810-10-20), purchased from Dharmacon. siRNAs were transfected using Lipofectamine-RNAiMAX (Life technologies, S.A., 13778) according to the manufacturer's instructions.

URI in INS-1 and INS-1E cells was knock-down using three different small interfering RNA (siRNA) against *Uri1* sequence (Origene, SR502040) and Lipofectamine2000 transfectant (Life technologies, 11668): Cells were plated at 70% confluence at transfection in 24-well plates. siRNAs 20 μM and Lipofectamine2000 were diluted in Opti-MEM transfection media (Life technologies), mixed for and incubated for 20 min and then applied to the cells on day of seeding and 24h onward. siGLO green transfection indicator (Thermo Scientific Dharmacon, D-001630-01-05) and was added as qualitative control of siRNA delivery to the nucleus. Cells were analyzed 48-hour post-transfection.

CVB4 Infections in Cells

Human Coxsackievirus B4 JVB strain was purchased from the American Type Culture Collection (ATCC VR-184#), was propagated in HEK293T cells and culture supernatants containing the viruses kept at –80°C. Non-infecting-CVB4 particles were prepared by incubating in 56°C water bath during 30 minutes.

Monolayers of INS-1 and INS-1E cultures set up in 24-well dishes with glass coverslips or in 6-well dishes were infected with CVB4 at MOI ranging from 50 to 0,001. Cells were collected after 24h incubation.

CVB4 Infection of Human Islets

150 to 200 human primary islets were cultured with CMRL-1066 media (Thermo Fisher Scientific) supplemented with 10% fetal bovine serum, l-glutamine, and penicillin/streptomycin and infected with 1×10^6 plaque-forming units of CVB4/100 islets by following previously reported procedures.²² Mock-infected islets were treated with media alone.

Flow Cytometry

Cells were trypsinized and 10^6 cells were harvested and washed in PBS two times. After final wash, cells were incubated in 70% ethanol overnight at 4°C. After washing twice in PBS, cells were incubated in 0.5 mL PBS containing 10 μg/ml RNase A, 50 μg/ml propidium iodide and 0.1 Triton x100 overnight in the dark at 4°C.

Pancreatic Insulin Content

Between a quarter to a half of pancreatic tail was placed in 5 mL of acid ethanol (1.5% HCl in 70% ethanol) overnight at –20°C. The day after, tissue was homogenized with a Precellys 24 tissue homogenizer (15 s x 2 power set to 5500 w) and incubated overnight at –20°C. Thereafter, samples were spun down at 2000 rpm for 15 min at 4°C. Supernatant was transferred to new tubes and stored at –20°C. 100 μL of acid ethanol extract were neutralized with 100 μL of Tris pH 7.5. Neutralized solution was diluted 1:500. Insulin content of samples was measured by enzyme-linked immunosorbent assay (ELISA) kit (Mercodia, 10-1249-01), following manufacturer's instructions. Analysis was done with Gene 5 software. Total protein content per sample was quantified with Bradford protein assay kit (Bio-Rad, 5000006) and bovine serum albumin (BSA) as standard protein. Optical density of samples and BSA was measured at 562nm using Gene 5 program.

Blood Parameters

Blood was collected from the heart of sacrificed mice and transferred to EDTA containing tubes for hemogram analysis using Abacus Junior Vet analyzer (Diatron, UM-AJV-01-276). Plasma was collected after 4000 rpm, 20 minutes at 4°C centrifugation and kept at –80°C until further analysis. Insulin and glucagon were measured by using kits as indicated in the [KEY RESOURCES TABLE](#).

FITC-Dextran Assay

For FITC/Dextran permeability assay mice were first starved for 12 hr and then given 60 mg/100 g of body weight of FITC/Dextran (46945, Sigma) dissolved in water by oral gavage as previously described.²⁴ Serum was collected 4 hr later and analyzed by Synergy HTX Multi-Mode Microplate Reader (BioTek) at the 485 nm excitation wavelength and 528 nm emission wavelength by using Gen5™ software (BioTek).

Immunoprecipitation

For immunoprecipitation of endogenous URI and estrogen receptor α (ER α), freshly harvested pancreases, MCF-7 or INS-1E cells were lysed in the following buffer (50 mM Tris-HCl pH.8, 100 mM NaCl, 1% NP-40, PMSF 50 μg/ml, 2 mM EDTA and 5% glycerol), supplemented with protease inhibitors. Immunoprecipitation was performed using 20 μL Protein A and/or G-Sepharose beads. Cell lysates were pre-cleared for 1 hour at 4°C using beads in absence of antibodies. Supernatant was then collected for input (whole cell extract, WCE) and for incubation with antibody at 4°C for 2 hours and then transferred to Protein A and/or G beads for additional 1 hour. Beads with bound proteins were washed 4 times in 1 mL immunoprecipitation buffer prior elution in 40 μL 2x Laemmli buffer.

Chromatin Immunoprecipitation

For chromatin immunoprecipitation (ChIP) assay, MCF-7 cells were cross-linked for 10 min at RT in 1% formaldehyde. Cross-linking reactions were stopped by adding 1.25 M glycine to a final concentration of 125 mM. Cells were centrifuged for 10 min at 4°C and then washed in cold PBS. Cells were lysed with 1 mL of lysis buffer-1 (50 mM HEPES-KOH, pH 7.5, 140 mM NaCl, 1 mM EDTA, 10% glycerol, 0.5% NP-40, 0.25% Triton X-100, 1 X protease inhibitor) followed by centrifugation at 4°C and resuspension of the pellet in lysis buffer-2 (10 mM Tris-HCl, pH 8.0, 200 mM NaCl, 1 mM EDTA, 0.5 mM EGTA, 1 X protease inhibitors). Finally, the pellets were resuspended in 1 mL of lysis buffer-3 (10 mM Tris-HCl, pH8.0, 100 mM NaCl, 1 mM EDTA, 0.5 mM N-lauroylsarcosine, 1 X protease inhibitors), and 100 μL of 10% Triton X-100 were added and sonicated for 20 min in a Covaris sonicator. The soluble fraction was quantified with Bradford, and 400 μg was used to immunoprecipitate the transcription factors and IgG's used as a control. Chromatin and antibody mixtures were incubated overnight at 4°C in total volume of 500 μL. Immunoprecipitated mixture was washed with a low salt buffer (20 mM Tris-HCl, pH 8.0, 150 mM NaCl, 2 mM EDTA, 0.1% SDS and 1% Triton X-100), followed by high salt buffer (20 mM Tris-HCl, pH 8.0, 500 mM NaCl, 2 mM EDTA, 0.1% SDS and 1% Triton X-100) and finally with LiCl wash buffer (10 mM Tris-HCl, pH 8.0, 250 mM LiCl, 1 mM EDTA, 1% Na-Deoxycholate and 1% NP-40). Samples were decross-linked by resuspending the beads in 210 μL of elution buffer (50 mM Tris-HCl, pH 8.0, 10 mM EDTA and 1% SDS), incubating at 65°C for 15 min and treating with 2.5 μL (from 32 mg/mL) of RNase A for 2 hours. Next, 4 μL of (20 mg/ml of stock) of Proteinase K was added and incubated at 55°C for 2 hours. DNA was extracted by phenol/chloroform/isoamylalcohol mixtures, washed with 80% EtOH and resuspended in 200 μL of TE buffer. This was followed by qRT-PCR. The specific primers used are listed below in [Table S3](#).

Cell Fractionation

6.106 INS-1E cells were lysed in 160 μ L Buffer C (10 mM HEPES pH 7.6, 3 mM MgCl₂, 40 mM KCl, 5% Glycerol, 0.5% NP-40, 2 mM DTT, 0.1 mg/ml PMSF 10 μ g/ml Aprotinin and 1X Protein inhibitor cocktail), vortexed 10 s, incubated 5 min at 4°C and checked under microscope. Subcellular fractionation were performed as previously described.⁸⁶ The resulting supernatant was saved and the pellet was washed with 120 μ L Buffer C. Both supernatants were combined and used as the cytoplasmic fraction for subsequent experiments. Pellet was washed another time with Buffer C and supernatant was discarded. Pellet was resuspended with 120 μ L Buffer N (10 mM HEPES-NaOH pH 7.9, 0.1 mM EDTA, 0.1 mM EGTA, 1.5 mM MgCl₂, 420 mM NaCl, 25% Glycerol, 0.5 mM DTT, 0.5 mM PMSF and 1X Protein Inhibitor Cocktail (Roche, 04693116001)). The lysate was vortexed for 10 s, placed for 10 min at 4°C and pelleted. Supernatant was used as nuclear fraction.

CAT Assay

Catalase activity in HEK293T cells was measured by the Catalase Activity Assay Kit (Abcam, ab83464) following manufacturer's instructions. Briefly, the catalase reacts with H₂O₂ to produce water and oxygen. The unconverted H₂O₂ reacts with probe to produce a product that can be measured colorimetrically at OD 570 nm.

Immunoblotting

Immunoblotting was performed from isolated cells, INS-1, INS-1E cells, HET293T cells, and different mouse organs i.e., spleen, kidney, colon, skin, ovaries, hypothalamus, heart and pancreas. Pancreas was removed from mice and pancreatic tail was directly frozen in liquid nitrogen. Tissues or cells were lysed in RIPA lysis buffer (10 mM Tris pH 7.5, 100 mM NaCl, 1 mM EDTA, 1 mM EGTA, 1 mM NaF, 20 mM Na₄P₂O₇, 2 mM Na₃VO₄, 0.1% SDS, 0.5% sodium deoxycholate, 1% Triton X-100, 10% glycerol and supplemented with 10 mg/ml proteases inhibitor aprotinin and 1mM PMSF) and tissues were lysed by homogenization using Precellys 24 Bead Mill homogenizer (Bertin Technologies) (15 s x 2 power set to 5500 w) and then clarified by centrifugation at 4°C and 10.000 g for 10 min. Protein concentration was measured by using the Bradford protein assay kit from Bio-Rad and BSA as standard protein. 1 mg/ml concentrated lysates were made by boiling the appropriate amount of protein lysates with 5X Laemmli buffer (10% SDS, 50% glycerol, 0.004% bromophenol blue in 0.2 M Tris-HCL of pH 7) and 0.1M Dithiothreitol (DTT) at 95°C, for 2 min. 10-30 μ g of protein lysates were subjected into SDS-PAGE gels, and transferred to nitrocellulose membranes. The membranes were blocked with 5% nonfat milk in Tris-buffered saline containing 1% Tween 20 for 1h at room temperature. Blots were immune-stained with indicated antibodies. Immunoblots were processed by ECL (2.5 mM Luminol, 0.4mM p-Coumaric Acid and Tris-HCl 0.1M, pH 8.5 for Luminol Solution and 0.02% hydrogen peroxide and Tris-HCl 0.1M, pH 8.5 for H2O2 solution; mixed 1 in 1 before revelation).

Immunohistochemistry

Pancreas was prepared by disposing the head of the pancreas on smoking paper and fixing it with 10% formalin along with the rest of the organs in paraffin cassettes. Samples were incubated overnight in formalin at room temperature and processed for paraffin embedding. Sections of 3 μ m were de-paraffinized, rehydrated and antigen retrieved by using 0.1 M sodium citrate buffer (pH 6.5). After blocking endogenous peroxidase using 3% H₂O₂ (in water) for 10 minutes, sections were then blocked with 1:200 goat serum in PBS/0.2% Triton for 1 hour at room temperature. Furthermore, sections were incubated with primary antibodies diluted in PBS/0.2% Triton overnight at 4°C. Slides were washed twice in PBS and Vectastain ABC kit (PK-4001 for rabbit; PK-4002 for mouse; PK-4005 for goat) was used for secondary antibody. Sections were washed twice in PBS and incubated with 3,3'-diaminobenzidine tetrahydrochloride (DAB) (Dako, K346811). For double staining, anti-Mouse IgG (whole molecule)-alkaline phosphatase antibody produced in goat (A3562, Sigma-Aldrich) and SIGMAFAST Fast Red TR/Naphthol AS-MX kit were used (F4648, Sigma-Aldrich). Counterstaining was performed with hematoxylin.

Immunofluorescence

For immunofluorescence, sections were directly blocked after deparaffinization and antigen retrieval with 1:200 goat serum and 5% BSA in PBS/0.2% Triton for 1 hour at room temperature. Incubation with primary antibodies in PBS/0.2% Triton was performed overnight at 4°C. After several washings in PBS, slides were incubated with Alexa488/555/647 conjugated secondary antibodies for 1 hour at room temperature, followed by DAPI (1 μ g/ml) staining. Mounting was done with fluorescent mounting media (DAKO, S3023). Quantification was performed either by counting the number of positive cells in a minimum of six 10X or 20X microscopic fields, the percentage of positive area or the mean fluorescence intensity of ROI using NIS-Elements AR.

Electron Microscopy

Samples were fixed with 2% v/v glutaraldehyde in 0.05 M sodium phosphate buffer (pH 7.2). Following isolation of suitable specimen blocks, the samples were rinsed three times in 0.15 M sodium phosphate buffer (pH 7.2) and subsequently post-fixed in 1% w/v OsO₄ in 0.12 M sodium phosphate buffer (pH 7.2) for 2-hour. The specimens were dehydrated in graded series of ethanol, transferred to propylene oxide and embedded in Epon according to standard procedures. Sections, approximately 60 nm thick, were cut with a Ultracut 7 ultramicrotome (Leica, Vienna, Austria) and collected on copper grids with Formvar supporting membranes (Ted Pella, 01700-F) stained with uranyl acetate (Agar scientific, AGR1260A) and lead citrate (Agar scientific, AGR1210), and subsequently examined with a Philips CM 100 Transmission EM (Philips, Eindhoven, the Netherlands), operated at an accelerating voltage of

80 kV and equipped with an OSIS Veleta digital slow scan 2k x 2k CCD camera. Digital images were recorded with the ITEM software package. Electron microscopy was performed by Klaus Qvortrup, Professor, MD, PhD, University of Copenhagen Faculty of Health and Medical Sciences, CFIM, Copenhagen, Denmark.

Bisulfite Sequencing

Unmethylated cytosines of DNA samples were converted to uracils by treating DNA with the EpiTect Bisulfite kit (QIAGEN, 59104), as recommended by the manufacturer. Fragments corresponding to Site 1 to 3 were amplified by PCR with Platinum Taq DNA Polymerase (Invitrogen, 10342020) and an annealing temperature of 60°C. Primer sequences are listed in Table S4. PCR products were cleaned up on NucleoFast PCR plates (Macherey-Nagel, 743100.10) and cloned on pGemT-easy (Promega, A1360). Plasmid colonies from each sample were sequenced and analyzed with BiQ Analyzer software as reported.⁸⁷

Genotyping

For genotyping, finger DNA was extracted by overnight incubation of fingers with 500 μ L of the cell lysis buffer (1% SDS, 0.1 M NaCl, 0.1 M EDTA, 0.05 M Tris (pH 8) and 400 μ g/ml of proteinase K). DNA obtained after saturated salt precipitation (5 M NaCl) was further precipitated using ice-cold isopropanol. DNA pellet was washed with 70% ethanol. Purified DNA was dried and resuspended in 200 μ L of distilled water. 1 μ L of DNA was used for genotyping as previously reported.^{28,29} Primers used for genotyping are listed in Table S5. Amplification products for *Lep* alleles were incubated with 10% cutsmart enzyme buffer and 1% of Ddel restriction enzyme overnight at 37°C before analysis on agarose gels.

qRT-PCR

For qRT-PCR, total RNA was extracted from frozen pancreas or different cell lines as described previously^{24,28,29} and qRT-PCR was performed with primers described in Table S6.

QUANTIFICATION AND STATISTICAL ANALYSIS

Statistical Analysis

Statistical analyses were performed using GraphPad Prism V5.0 software. Statistical significance (p) ($p \leq 0.05 = *$, $p \leq 0.01 = **$ and $p \leq 0.001 = ***$) between the means of two groups was determined using unpaired two-tailed Student's t test, two-way ANOVA, Mantel-Cox test, Mann Whitney test or linear regression analysis as indicated in the Figure legends. Results are expressed as the mean value \pm Standard Error of the Mean (SEM). Kaplan Meier curve for the survival analysis of mice was used. WB are representative of at least three independent experiments. IF, H&E and IHC are representative of at least three independent mice. Quantification of IF, H&E and IHC are performed in at least three independent mice. In the case of the experiments *in vitro*, at least three independent experiments are performed and quantified. For the *in vivo* experiments, at least three mice per group are used. "n" represents number of mice or human samples used in each experiment, as indicated in Figure Legends. "N" represents number of independent experiments performed with cells, as indicated in Figure Legends.

Image Analysis

At least six images per slide were taken at 5 – 10 – 20 X magnifications and quantified using color de-convolution, a colocalization finder and image analysis tools available in ImageJ 1.7v software. As well, different macros were developed by the authors to quantify immunofluorescence.

To quantify the proportion of different cells in the islets, number of positive cells were counted and normalized to total cell number per islet.

To quantify β cell density, number of nuclei was counted manually and normalized to the area of the islets in μm^2 .

Scoring Signal in Human Samples

URI and Insulin scoring was performed as follows: 0 corresponds to no signal in the pancreatic islet ($n = 20$); 1 to weak signal ($n = 23$); 2 to moderate signal ($n = 25$); 3 to robust signal ($n = 11$); 4 to strong signal ($n = 1$).

For PDX1 and DNMT1 quantification, percentage of positive nuclei in the pancreatic islets of all the islets present in each sample were counted.

β cell Mass Quantification

Beta cell mass (mg per pancreas) was calculated by multiplying the average of relative insulin-positive area of 3 slides distant of 50 μm (the percentage of insulin positive area over total pancreas area) by pancreas weight.